SSC-SR-1024

The Superconducting Super Collider

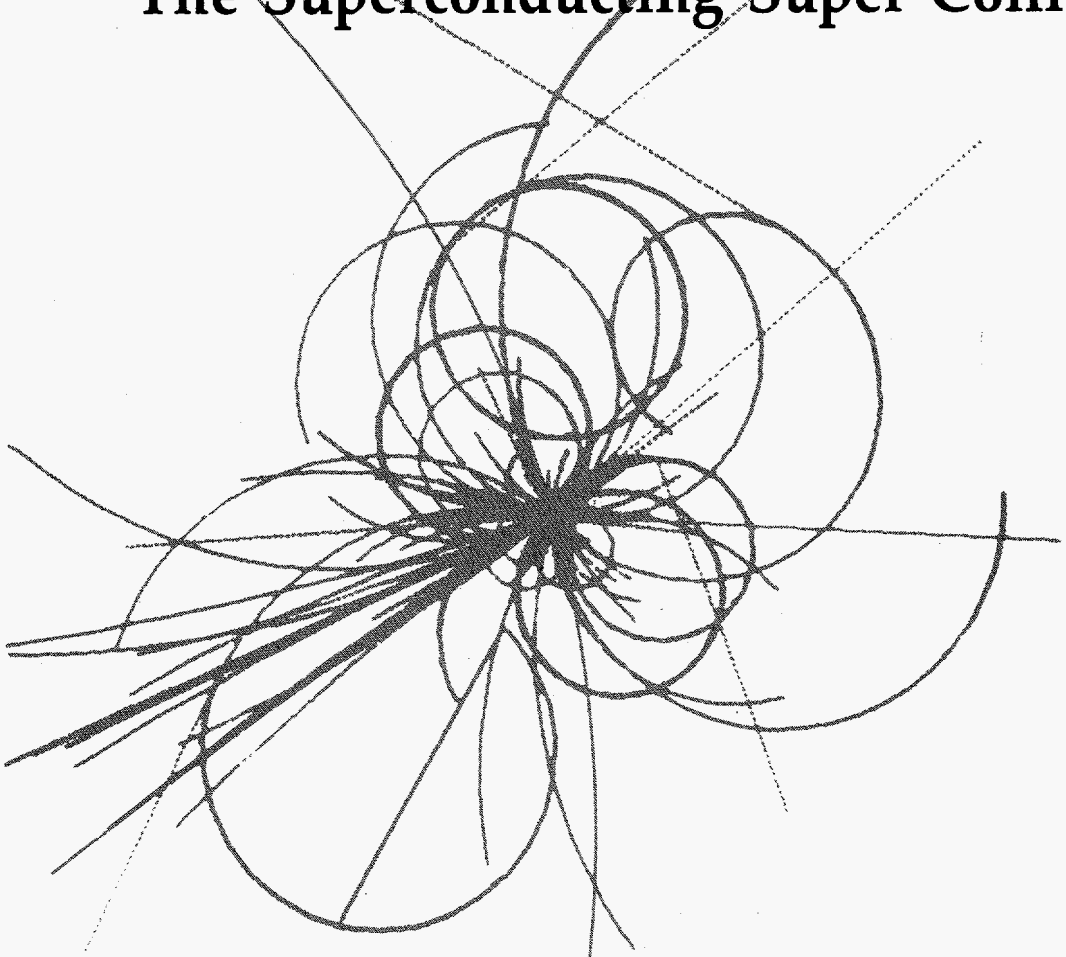

Optimization of the Cell Lattice Parameters for the SSC

Cell Lattice Study Group
SSC Central Design Group

October 15, 1986

APPROVED FOR RELEASE OR
PUBLICATION - O.R. PATENT GROUP
BY.....DATE. 4/3/95

DISTRIBUTION OF THIS DOCUMENT IS UNLIMITED

MASTER

SSC-SR-1024

OPTIMIZATION OF THE CELL LATTICE PARAMETERS FOR THE SSC

Cell Lattice Study Group

SSC Central Design Group*
c/o Lawrence Berkeley Laboratory
Berkeley, California 94720

DISCLAIMER

This report was prepared as an account of work sponsored by an agency of the United States Government. Neither the United States Government nor any agency thereof, nor any of their employees, makes any warranty, express or implied, or assumes any legal liability or responsibility for the accuracy, completeness, or usefulness of any information, apparatus, product, or process disclosed, or represents that its use would not infringe privately owned rights. Reference herein to any specific commercial product, process, or service by trade name, trademark, manufacturer, or otherwise does not necessarily constitute or imply its endorsement, recommendation, or favoring by the United States Government or any agency thereof. The views and opinions of authors expressed herein do not necessarily state or reflect those of the United States Government or any agency thereof.

October 15, 1986

*Operated by Universities Research Association for the Department of Energy.

DISTRIBUTION OF THIS DOCUMENT IS UNLIMITED

Cell Lattice Study Group

A. Chao, SSC/CDG (Chairman)
E. Forest, SSC/CDG
A. Garren, SSC/CDG
M. Harrison, SSC/CDG/Fermilab
D. Johnson, SSC/CDG/Fermilab
H. Lee, SSC/CDG/Los Alamos
S.Y. Lee, BNL
B. Leemann, SSC/CDG
H. Mais, DESY
R. Meller, SSC/CDG
D. Neuffer, Los Alamos
S. Peggs, SSC/CDG
J. Peterson, SSC/CDG
W. Scandale, CERN
L. Schachinger, SSC/CDG
R. Talman, Cornell
M. Tigner, SSC/CDG

DISCLAIMER

Portions of this document may be illegible in electronic image products. Images are produced from the best available original document.

Chapter		Page
I	Introduction	1
II	Cell Lattices	5
III	Needed Aperture	11
IV	Magnet Errors	15
V	Calculated Aperture	19
VI	The Trade Off Curves	25
VII	Cost Model	29
VIII	Additional Considerations	35
IX	Conclusions	45
Appendix A	Details of the Cost Model	49
Appendix B	Example of a 90° Cell SSC Lattice	53

CHAPTER 1

Introduction

The SSC lattice consists of two clusters of interaction regions connected by two arcs, each consisting of a long string of cells. The cell lattice parameters are important in that they enter the evaluation of the linear aperture* on the one hand and the cost on the other. In the Conceptual Design Report (CDR)[1] and the preceding aperture evaluation efforts,[2] attempts were made to optimize the SSC design taking into consideration the interplay among the cell length, the linear aperture, the magnet coil diameter, and the cost. These results were subsequently used in the CDR.

The optimization process has now been repeated by a study group organized by the Central Design Group (CDG). There are basically two reasons for the repetition:

1) The cost model and the analytical and numerical techniques to evaluate linear aperture have been improved since the pre-CDR studies, allowing more accurate cost and linear aperture calculations.
2) In the previous studies, the betatron phase advance per cell--another important cell lattice parameter--was fixed at 60 degrees. An alternative value of phase advance would have been 90 degrees. Preliminary results were obtained for 90-degree cells, but a systematic optimization study was missing except for an indication that, under the condition that the cost is held fixed, the difference between 60- and 90-degree cells was small[3] and was considered to be below the noise level using the then available tools. The more accurate cost model and linear aperture calculation now have allowed us to review this issue more carefully.

*Linear aperture is the aperture within which particle motion is approximately linear. The cell design must permit sufficient linear aperture for routine beam operations. For more discussions, see Refs. 1 and 2.

The study group thus held a meeting on August 13, 1986, at Lawrence Berkeley Laboratory to discuss the issues involved and to prepare for a later Cell Lattice Workshop, which was held on September 17-18, 1986, at LBL. Results of the study are given in this report. Although the precise value of the magnet coil diameter may still require later inputs, based on this study it has been possible for the group to make concrete recommendations.

The structure of this report is as follows: Chapter II describes the 90- and 60-degree cell lattices for various cell lengths. Chapter III specifies the needed linear aperture, including off-momentum requirements, for each of these lattices. This needed linear aperture is normalized with respect to the CDR case. Magnet errors depend on the coil diameter; the expected magnet multipole errors for a range of coil diameters are given in Chapter IV. Having specified the cell lattice and the magnet errors, analytic and tracking techniques are applied to calculate the linear aperture in Chapter V. The calculated aperture and the needed one are then compared in Chapter VI to obtain two curves, one for 60-degree cells and one for 90-degree cells, which represent the trade-off between cell length and magnet coil diameter. Along a trade-off curve, the calculated and the needed apertures are equal. Any point along the trade-off curve therefore represents a viable SSC design as far as the linear aperture is concerned. A cost model is described in Chapter VII which gives the cost of the SSC as a function of cell length and magnet coil diameter for 60- and 90-degree designs. There are a few additional effects, other than the linear aperture, which are influenced by the choice of cell parameters and coil diameter. Examples are the dynamic aperture, the tune shifts caused by the persistent currents and the systematic multipole tolerances and the number of needed correction systems, the influence of beam pipe size on the various collective effects, and the interaction region lattice design. Discussions of these additional considerations are described in

Chapter VIII. Having obtained the cost model, the cheapest design along the trade-off curve is then identified to be the optimum SSC design. These discussions are given in the concluding Chapter IX.

The CDR has 60-degree cells with five dipole magnets, each 16.54 meters long, per half cell. The main recommendation of this study is to adopt 90 degree cells with six dipole magnets (of the same length) per half cell for the SSC arc design. The improvements over the CDR are again not overwhelming, but with the more accurate calculations the relative difference is believed to be real, i.e. above the noise level. This change, if adopted, will cause numerous small changes on the conceptual design, including lattice design, engineering design and cost of various systems, and conventional facilities.

CHAPTER II

Cell Lattices

The first step in evaluating the various cell configurations consists of calculating the cell lattice parameters associated with each configuration. The method chosen to do this is as follows:

1) For a given number of dipoles per half cell N, the half cell length is given by

   L = N • dipole + quadrupole + spool piece + magnet interconnections (1)

   For the case of the CDR, N = 5, the dipole, quadrupole, spool piece, and the effective lengths are 16.54 m, 3.32 m, 4.52 m, and 5.46 m respectively, giving a half cell length of L = 96 m. In this study, we have fixed the unit dipole length. The variation of cell length is obtained by varying N.

2) For given phase advance per cell μ, the focal length f of the quadrupole in this cell is given by

$$\sin \frac{\mu}{2} = \frac{L}{2f} , \qquad (2)$$

   where $f = \frac{B\rho}{B'\ell}$. Using a value of 212 T/m at 20 TeV for B' then determines the length of the quadrupole, ℓ.

3) The spool piece length is calculated by assuming that the change in length of the correction element package is defined by the needed sextupole strength to correct the chromaticity of this lattice. The ring-wide chromaticity is assumed to consist of a constant value from the interaction regions plus the natural chromaticity of the cells. The contribution to sextupole length required to correct for the cell chromaticities is approximately proportional to $(\sin \mu/2)^3/L^3$.

4) The cell length is then recalculated with the new quadrupole and spool piece lengths and steps 1 to 3 are iterated until the solution converges. Typically it requires 4 iterations to converge to within 1 cm.

After the cell length is defined, the lattice parameters are evaluated according to the thin lens formulae

$$\beta_{max} = 2L \frac{1 + \sin\frac{\mu}{2}}{\sin \mu}$$

$$\beta_{min} = 2L \frac{1 - \sin\frac{\mu}{2}}{\sin \mu}$$

$$\eta_{max} = \frac{L\theta}{\sin^2 \frac{\mu}{2}} [1 + \frac{1}{2} \sin \frac{\mu}{2}] \qquad (3)$$

$$\eta_{min} = \frac{L\theta}{\sin^2 \frac{\mu}{2}} [1 - \frac{1}{2} \sin \frac{\mu}{2}] ,$$

where θ is the half cell bend angle.

The results of the calculation are given in Figs. 1 and 2 which show the cell parameters as a function of N, the number of dipoles per half cell, for 60- and 90-degree phase advances. Increasing the phase advance per cell has very little effect on β_{max} but produces a substantial reduction in β_{min}, η_{max}, and η_{min}.

The half cell length for both phase advances is shown in Fig. 3, the stronger focussing results approximately a 5 m increase in cell length for the same number of dipoles. The corresponding change in machine circumference is shown in Fig. 4, which assumes that the interaction regions remain the same and the arcs are adjusted so as to preserve the overall 2π bending. The number of half cells per ring and packing factors are shown in Fig. 5.1 and 5.2. The number of half cells is given by the total number of dipoles in the ring (3840) divided by the number of dipoles per half cell. The packing

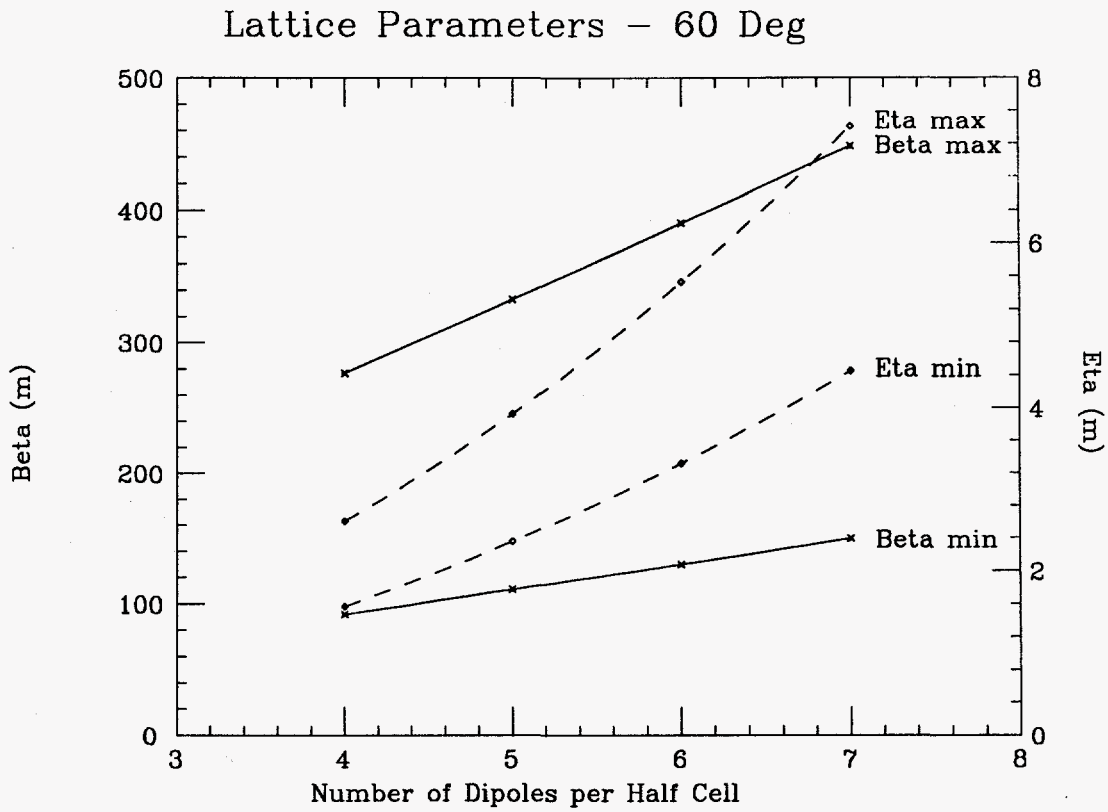

Fig. 1 Lattice parameters β and η for 60° normal cells as a function of the number of dipoles per half cell.

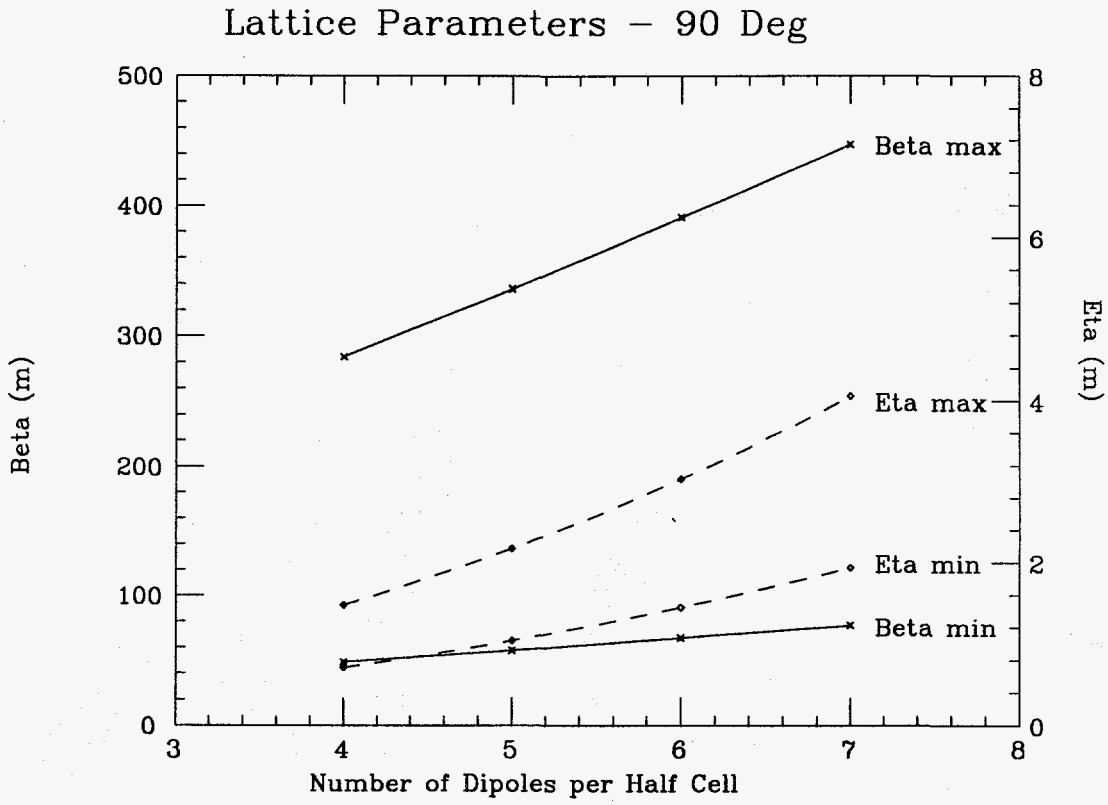

Fig. 2 Lattice parameters β and η for 90° normal cells as a function of the number of dipoles per half cell.

factor is calculated for the whole ring and is defined by the total effective bend length (3840 x 16.54 m) divided by the machine circumference and as such reflects the effect of the interaction regions as well as the cell parameters.

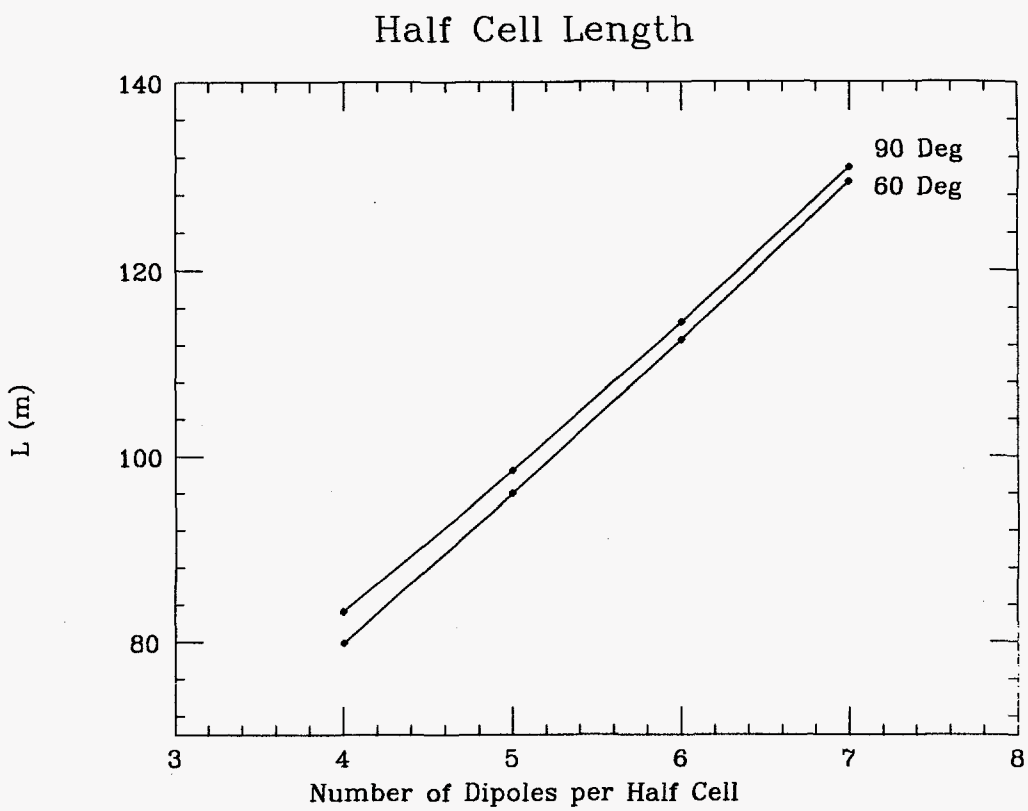

Fig. 3 Normal cell half length as a function of the number of dipoles per half cell.

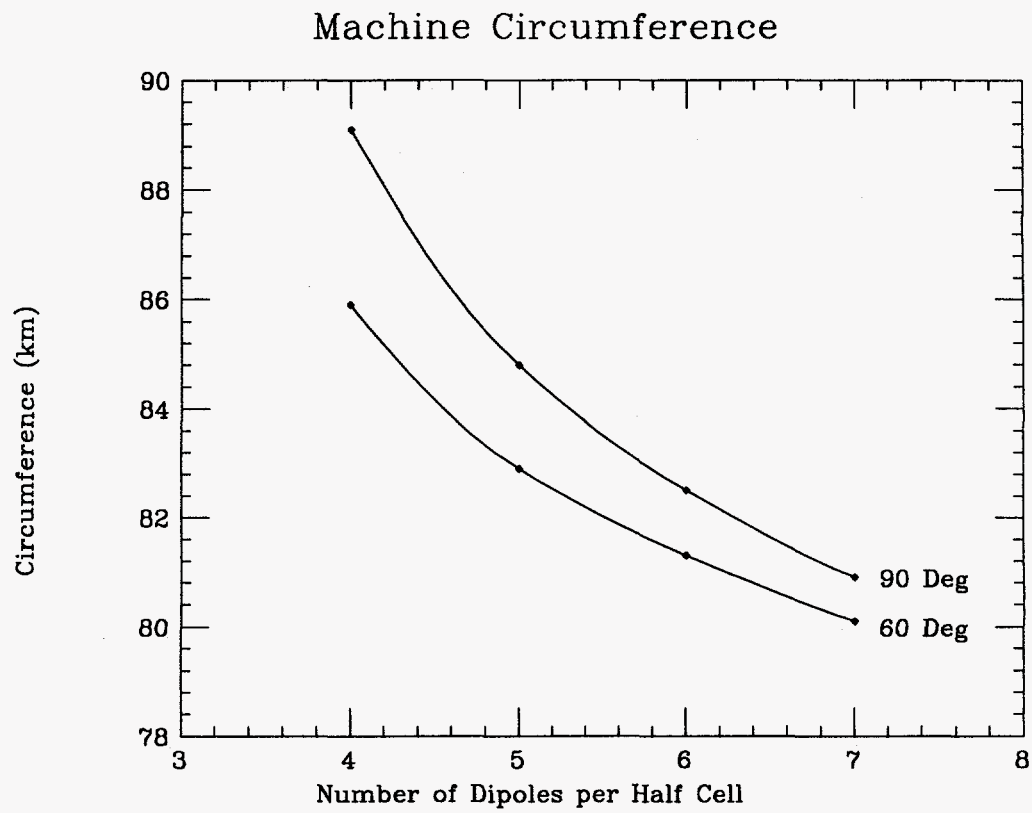

Fig. 4 Total machine circumference as a function of the number of dipoles per half cell.

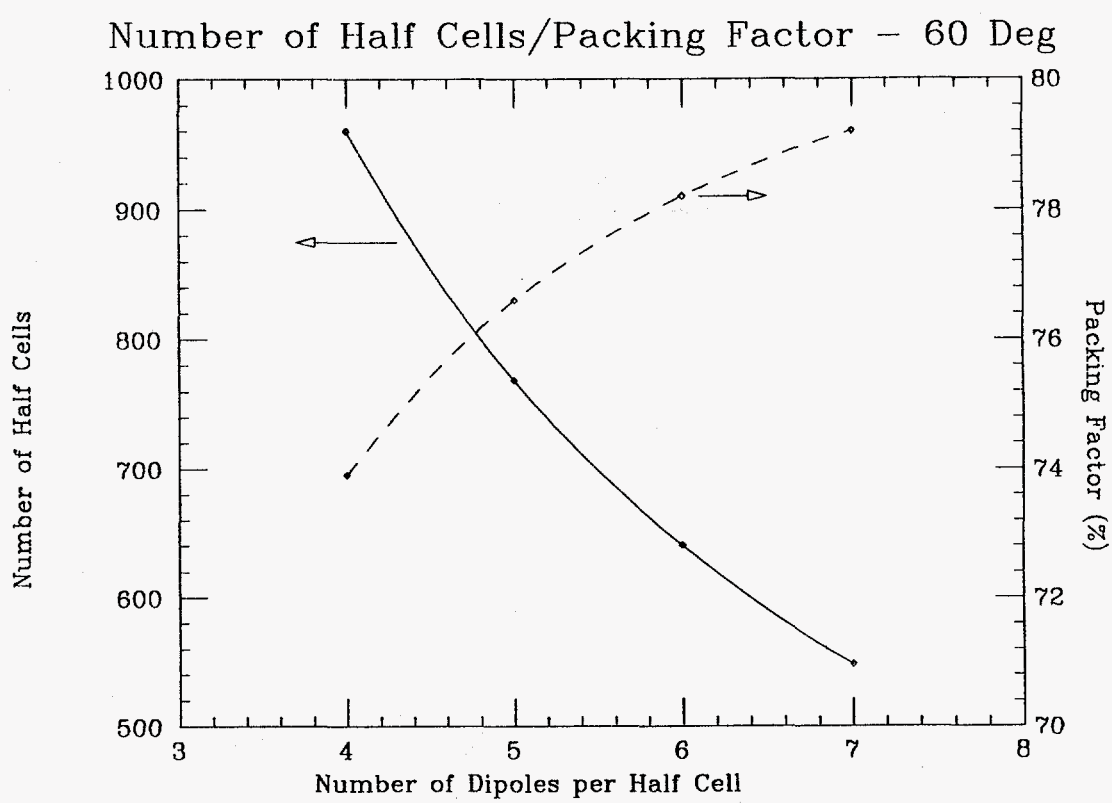

Fig. 5 Total number of half cells and overall machine packing factor as a function of the number of dipoles per half cell.

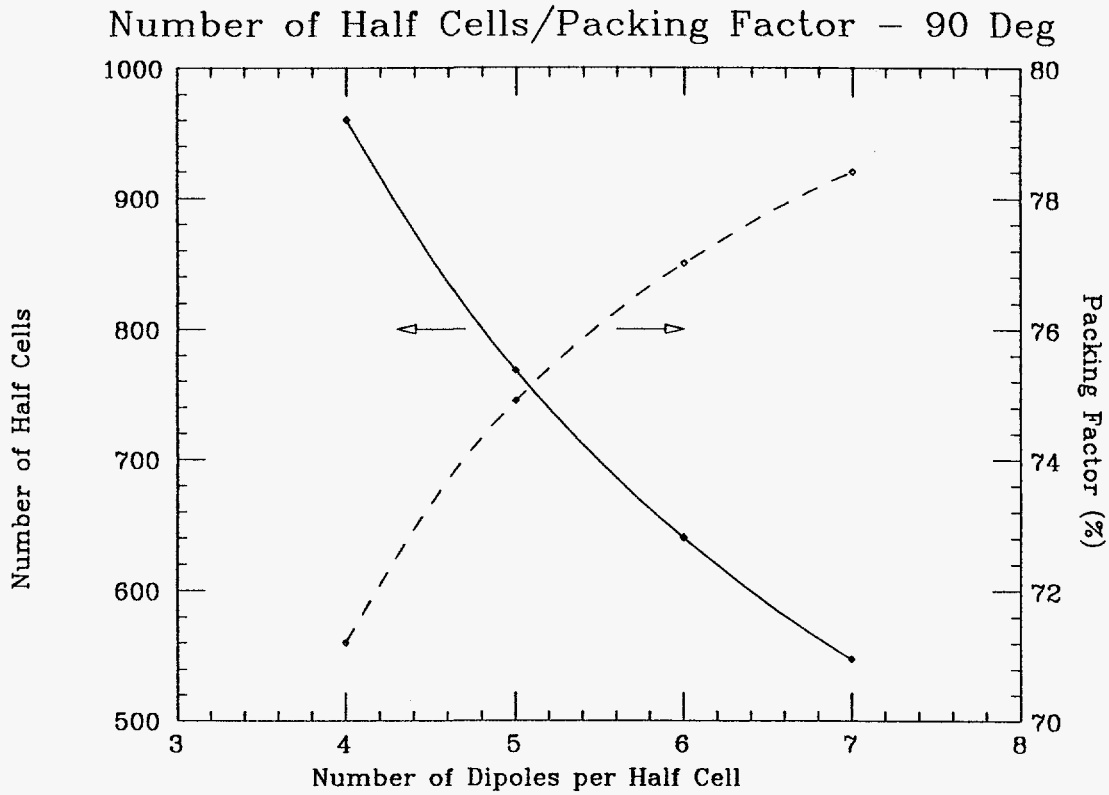

Fig. 5.2 Total number of half cells and overall machine packing factor as a function of the number of dipoles per half cell.

CHAPTER III

Needed Aperture

The aperture needed for beam storage and operation depends on the half cell length L and phase advance per cell μ. In general, a lattice with stronger focussing requires a smaller aperture for the beam. As in the CDR,[1] we identify two types of apertures, the linear aperture and the dynamic aperture, and it is the linear aperture that is regarded as the primary aperture requirement.

In the following analysis, the CDR aperture is defined as the normalization point. The CDR case (μ = 60 degrees, 5 dipoles per half cell, L = 96 m) is thus defined to be the standard for which the needed linear aperture is exactly equal to the achieved one. What will be obtained is a curve that shows the percentage variation of the needed linear aperture, relative to the CDR case, with respect to L and μ.

To obtain this curve, the needed linear aperture radius is first decomposed into four components. Each component has its own scaling with the cell lattice parameters. These four components are

1) Ninty-five per cent of the beam is contained in a beam size of $\sqrt{6}\,\sigma$, which for the CDR is 1.35 mm at β_{max} in the cells. This component scales with $\sqrt{\beta_{max}}$.
2) Residual betatron oscillation during injection can be as large as 1.5 mm in the CDR case. This requirement on linear aperture scales as $\sqrt{\beta_{max}}$.
3) Closed orbit distortions at β_{max} in the cells have rms value of 0.43 mm for the CDR case. The corresponding linear aperture requirement is taken to be 3 times the rms value, i.e., 1.29 mm. On the basis of the orbit correction scheme proposed in the CDR and keeping the rms misalignment of quadrupoles, dipoles, and the beam position monitors the same, it is found

that when the phase advance is increased to 90 degrees, the orbit distortion requirement decreases to 1.16 mm. However, the orbit distortion remains the same as cell length is changed in both the 60- and 90-degree cases.

4) Miscellaneous effects such as lattice mismatching, and power supply ripples and noises also contribute a small linear aperture requirement. For the CDR case, this is taken to be 0.52 mm. Half of this component is scaled with $\sqrt{\beta}_{max}$ and the other half is scaled with η_{max}.

The four components are added linearly to give the total needed linear aperture. (Reference 2 used a somewhat different recipe to obtain the linear aperture, but the final result does not change significantly.) Figure 6 shows the needed linear aperture as a function of cell length and phase advance. The percentage variation relative to the CDR case is shown using the scale on the left-hand side, while the absolute values are shown using the scale on the right.

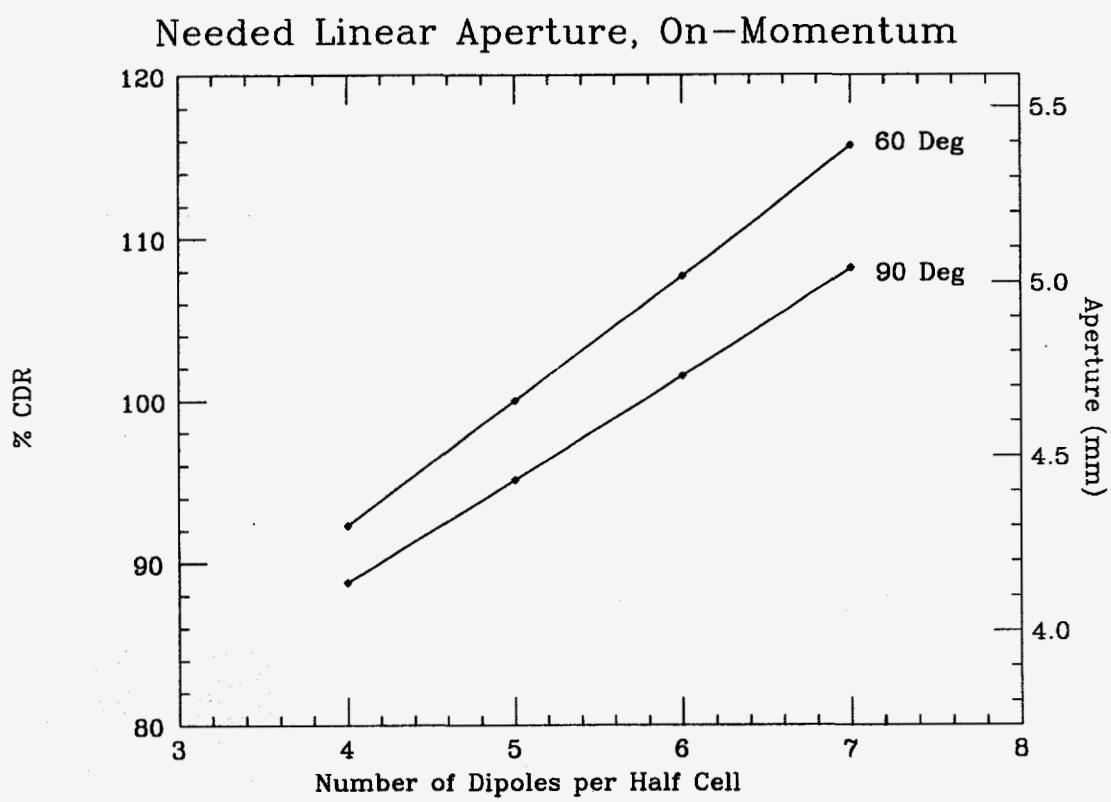

Fig. 6 Needed linear aperture for injection for a beam with $\delta = \Delta E/E = 0$ as a function of the number of dipoles per half cell.

As we will see later, the achieved linear aperture for the CDR case of 60-degree and five magnets per half cell is actually 9.9 mm, which is larger than the value 4.7 mm obtained by reading the scale on the right-hand side of Fig. 6. Since the extra aperture is necessary as a safety margin, the needed linear aperture for the CDR case is re-normalized to be 9.9 mm. The other cases are then obtained by the percentage scale on the left-hand side of Fig. 6.

The needed linear aperture shown in Fig. 6 is for on-momentum particles. For off-momentum particles, the needed linear aperture depends on the momentum error being considered. For extreme off-momentum particles with a value of $\delta = \Delta E/E = 10^{-3}$, the residual betatron oscillation requirement is removed. The resulting needed linear aperture, as a function of cell lattice parameters, is shown in Fig. 7. It is also shown as a percentage of the needed on-momentum linear aperture for the CDR case.

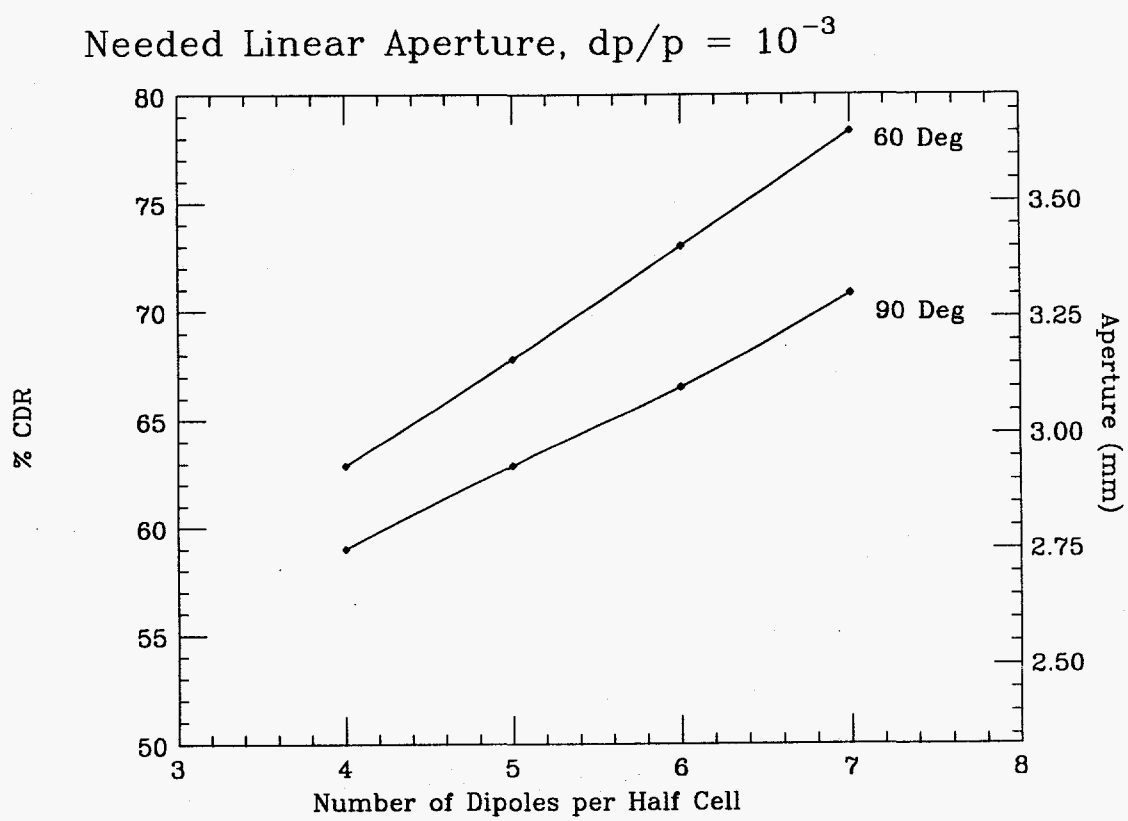

Fig. 7 Needed linear aperture for injection for a beam with $\delta = 10^{-3}$ as a function of the number of dipoles per half cell.

It is believed that the on-momentum linear aperture requirement, shown in Fig. 6, should be applied to off-momentum particles up to $\sqrt{6}\ \sigma_\delta$, which for the SSC has the value of 4.3×10^{-4}. In fact, this off-momentum requirement has been carried out in the following study of linear aperture evaluation. Although regarded important, it was found that this off-momentum requirement does not have any significant impact on the actual results. The details of this part of the study are therefore not included in this report.

CHAPTER IV

Magnet Errors

The rms variation of random magnetic multipoles for the several magnet coil sizes were scaled from the values for the CDR case that are listed in Ref. 4. The scaling equation for $n \geq 2$ is

$$\sigma(a_n) \text{ and } \sigma(b_n) \propto d_c^{-(n+\frac{1}{2})}, \tag{4}$$

where d_c is the inner diameter of the magnet coil package.

The resulting estimates of the rms variations in the multipole strengths to be expected in the dipoles with d_c = 3.5, 4.0, 4.5, and 5.0 cm are listed in Table 1. The estimates for the 4.0 cm case are simply those listed in Ref. 4. The same data are displayed also in Figs. 8.1 and 8.2.

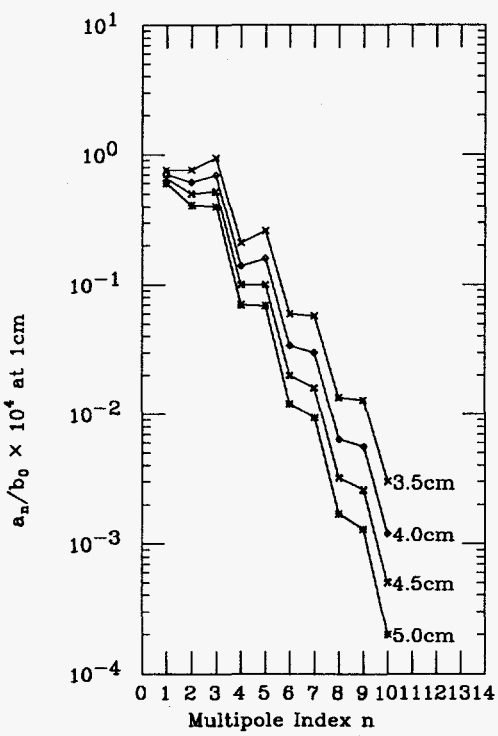

Figure 8.1

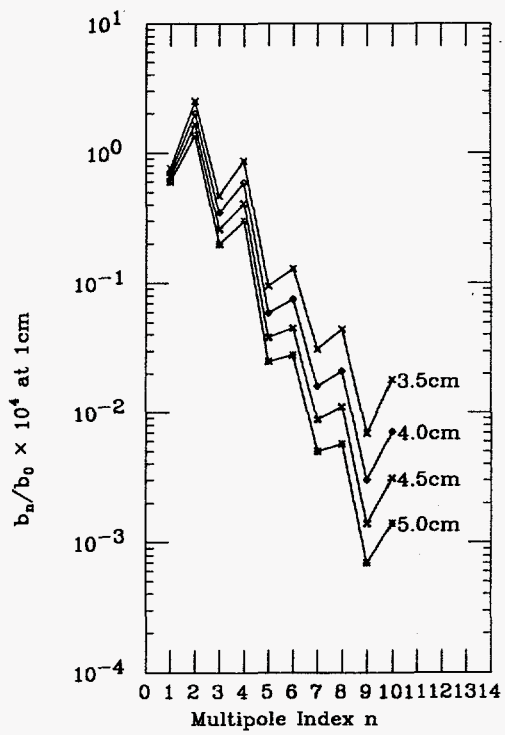

Figure 8.2

Fig. 8 RMS variations in the skew (Fig. 8.1) and the normal (Fig. 8.2) multipole strengths projected for dipoles with coil diameters 3.5, 4.0, 4.5, and 5.0 cm.

In the linear aperture evaluation to be described later, the random a_1 and b_1 multipoles are not included. These errors cause linear distortion of the lattice, which can be compensated by the correction elements.[1] Furthermore, the random b_2 used in aperture evaluation has been reduced by a factor of 5. This reduction is adopted assuming the "binning" corrections[5] have been applied, using 7 bins.[6] These changes made for aperture evaluation are listed in parentheses in Table 1.

Table 1

Estimated rms variations in the random mutipole strengths anticipated for SSC dipoles having coil i.d.s of 3.5, 4.0, 4.5, and 5.0 cm. Units are 10^{-4} of the dipole field at 1.0 cm.

Multipole	d_c=3.5 cm	d_c=4.0 cm	d_c=4.5 cm	d_c=5.0 cm
a_1	0.76 (0)	0.70 (0)	0.65 (0)	0.60 (0)
b_1	0.76 (0)	0.70 (0)	0.65 (0)	0.60 (0)
a_2	0.76	0.61	0.50	0.41
b_2	2.50 (0.625)	2.01 (0.402)	1.65 (0.33)	1.37 (0.274)
a_3	0.94	0.69	0.52	0.40
b_3	0.47	0.35	0.26	0.20
a_4	0.21	0.14	0.10	0.070
b_4	0.87	0.59	0.41	0.30
a_5	0.26	0.16	0.10	0.069
b_5	0.095	0.059	0.038	0.025
a_6	0.060	0.034	0.020	0.012
b_6	0.13	0.075	0.045	0.028
a_7	0.058	0.030	0.016	0.0094
b_7	0.031	0.016	0.0088	0.0050
a_8	0.0134	0.0064	0.0032	0.0017
b_8	0.044	0.021	0.011	0.0057
a_9	0.0128	0.0056	0.0026	0.0013
b_9	0.0069	0.0030	0.0014	0.0007
a_{10}	0.0030	0.0012	0.0005	0.0002
b_{10}	0.018	0.0071	0.0031	0.0014

CHAPTER V

Calculated Aperture

Given the lattice and the magnet errors, the linear aperture can be calculated either analytically[7] or by numerical particle tracking.[8] In the following, the linear aperture A_L is defined to be

$$A_L = \sqrt{\beta_{max}(\varepsilon_x + \varepsilon_y)} \ , \tag{5}$$

where β_{max} is the maximum β-function in the cells and the emittances ε_x and ε_y, taken to be equal by the initial conditions, are determined by requiring the smear to be less than 10%. The smear is defined by

$$S = \frac{2}{3} \max \left[\frac{\max A_x - \min A_x}{(\max A_x + \min A_x)} \ , \ \frac{\max A_y - \min A_y)}{(\max A_y + \min A_y)} \right] , \tag{6}$$

where max $A_{x,y}$ and min $A_{x,y}$ are the maximum and minimum x and y invariant amplitudes. In a tracking simulation, they are obtained typically by 400 turns of tracking.

To calculate the smear, the test lattice of the entire ring is obtained as follows. Given the unit cell structure, sufficient number of unit cells are connected together to form the two arcs. Magnets in these cells have errors as described in Table 1. The straight sections between the two arcs do not contribute directly to the aperture evaluation. Their only effect included in the simulation is their contribution to the natural chromaticities, whose correction require stronger settings of the chromaticity sextupoles. For this purpose, each straight section is represented as a string of unit cells whose dipoles do not contain errors and whose contribution to chromaticities equals that from a low-β insertion. This simplification is not expected to affect the aperture evaluation.

In the analytic calculation,[7] the rms smear is obtained

$$S_{rms} = 1.56 \max \left[\frac{\langle \Delta J_x^2 \rangle^{1/2}}{2J_x}, \frac{\langle \Delta J_y^2 \rangle^{1/2}}{2J_y} \right], \tag{7}$$

where $J_{x,y}$ are the linear invariants of the two degrees of motion. The numerical factor on the right-hand side of Eq. (7) is an empirical factor found to relate the two definitions (7) and (6) numerically. Equation (6) remains the adopted definition; however, having introduced the numerical factor, Eq. (7) gives the value of the smear rather accurately over the region of interest.

The advantage of having an analytical calculation is that the results over a wide range of parameters can be obtained quickly. Spot checking by particle tracking using the program RACETRACK has been performed on several cases to convince ourself that these results are reliable.[8] Excellent agreements were obtained in cases studied. Tracking also provided information on the spread of the smear value due to different detailed arrangement of the magnet errors through the dependence on random number seeds. The result of these studies are summarized in Tables 2.1 to 2.4. The same results are also given as Figs. 9.1 to 9.4.

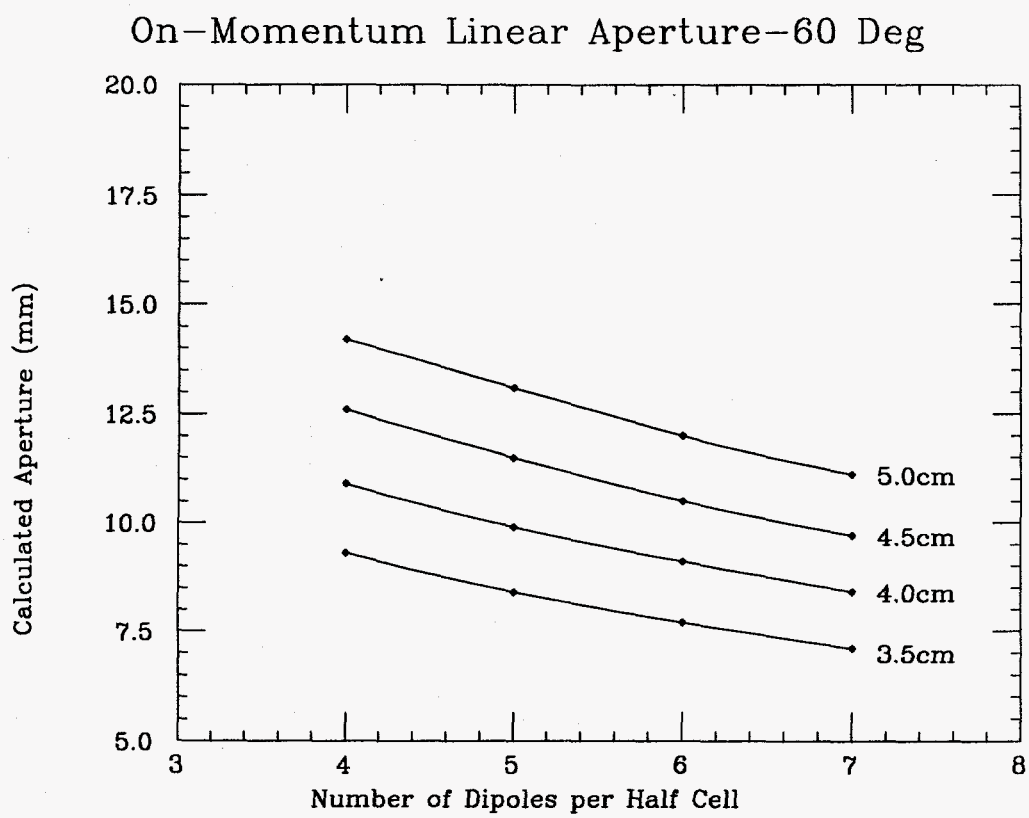

Figure 9.1

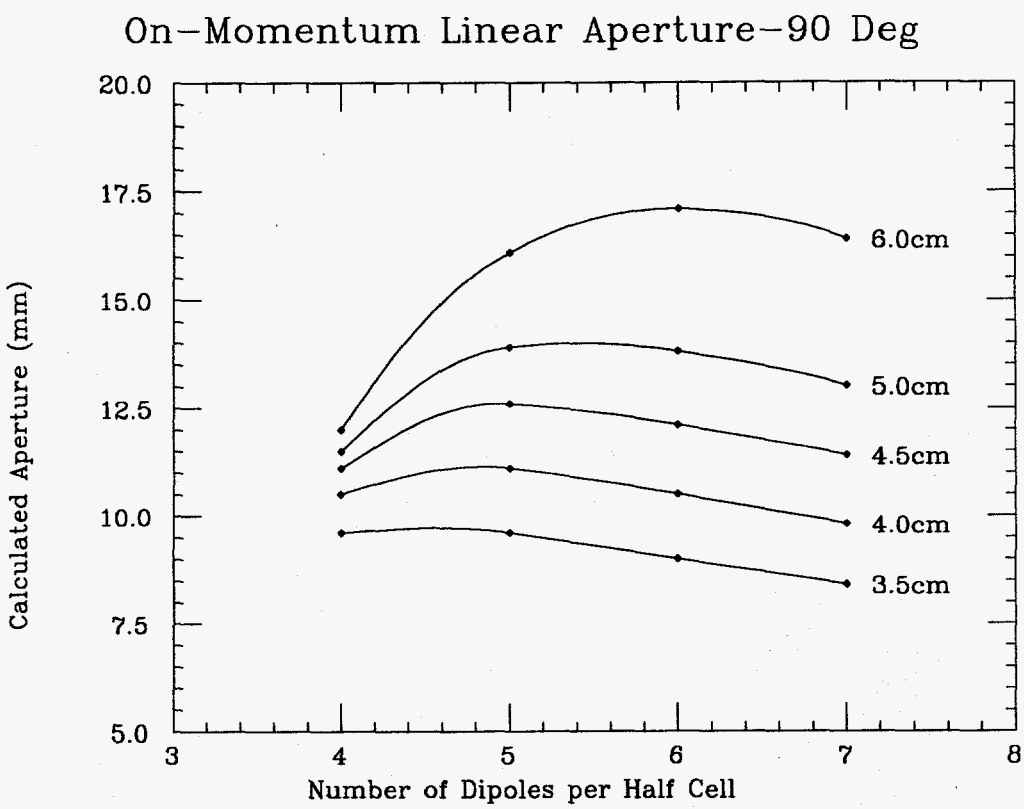

Figure 9.2

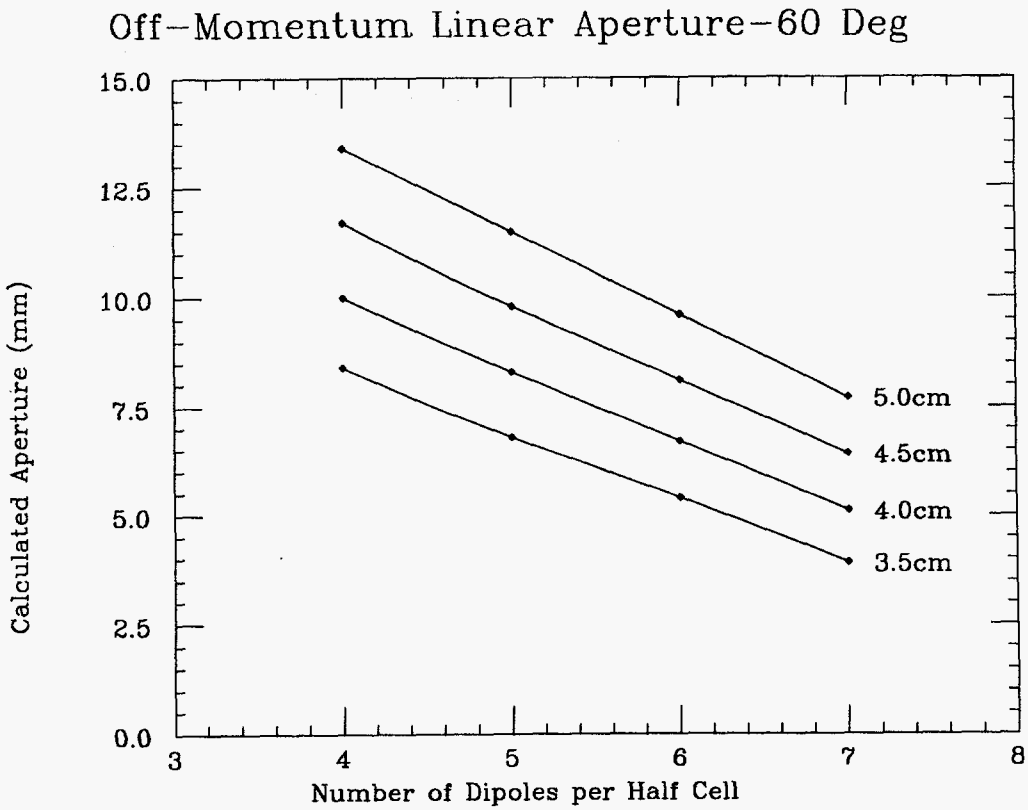

Figure 9.3

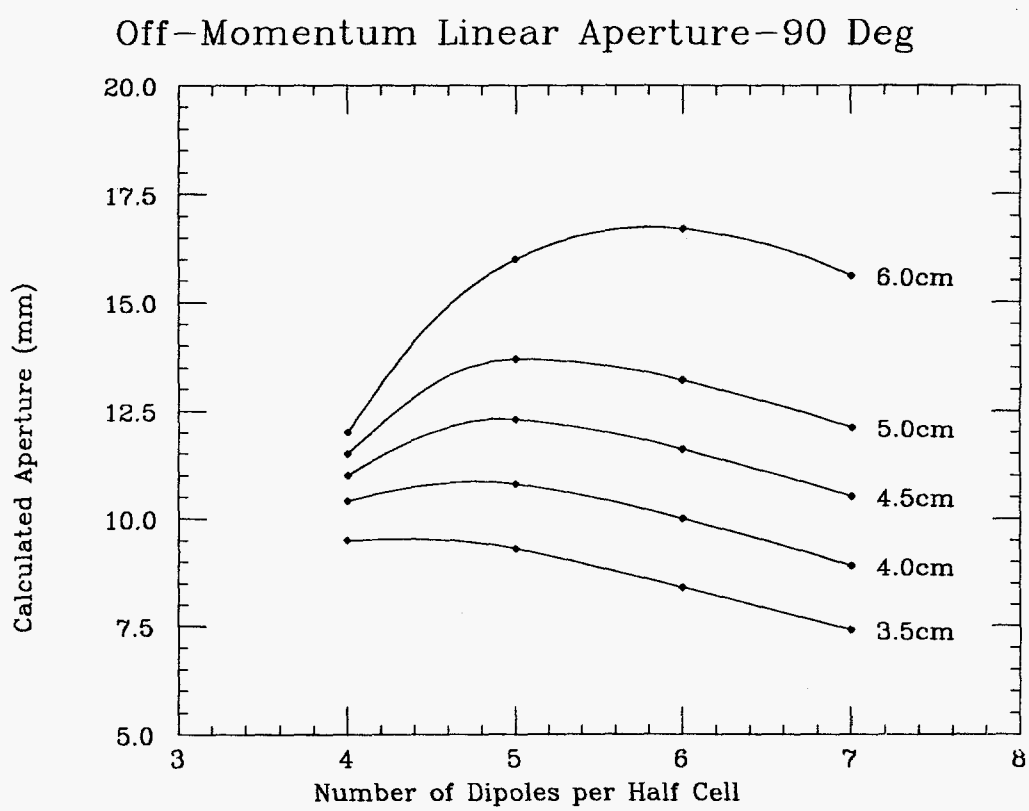

Figure 9.4

Fig. 9.1 - 9.4 Calculated available linear apertures for 60° and 90° cells, with $\delta = 0$ and $\delta = 10^{-3}$, for different dipole coil winding diameters as a function of the number of dipoles per half cell.

Table 2.1

Analytically calculated linear aperture (in mm) for various cases of cell structure and magnet coil diameter. Phase advance per cell is 60 degrees and the linear aperture is for on-momentum particles.

coil diameter	# of dipoles per half cell 4	5	6	7
3.5 cm	9.3	8.4	7.7	7.1
4.0 cm	10.9	9.9	9.1	8.4[a]
4.5 cm	12.6	11.5	10.5	9.7
5.0 cm	14.2	13.1	12.0	11.1

Table 2.2

Analytically calculated linear aperture (in mm) for various cases of cell structure and magnet coil diameter. Phase advance per cell is 90 degrees and the linear aperture is for on-momentum particles.

coil diameter	# of dipoles per half cell 4	5	6	7
3.5 cm	9.6	9.6	9.0	8.4
4.0 cm	10.5[a]	11.1	10.5[a]	9.8[a]
4.5 cm	11.1	12.6	12.1	11.4
5.0 cm	11.5	13.9	13.8	13.0
6.0 cm	12.0	16.1	17.1[a]	16.4

[a] Extensively checked against tracking with multiple random number seeds.

Table 2.3

Analytically calculated linear aperture (in mm) for various cases of cell structure and magnet coil diameter. Phase advance per cell is 60 degrees and the linear aperture is for particles with $\delta = 10^{-3}$.

coil diameter	# of dipoles per half cell 4	5	6	7
3.5 cm	8.4	6.8	5.4	3.9
4.0 cm	10.0	8.3	6.7	5.1[a]
4.5 cm	11.7	9.8	8.1	6.4
5.0 cm	13.4	11.5	9.6	7.7

Table 2.4

Analytically calculated linear aperture (in mm) for various cases of cell structure and magnet coil diameter. Phase advance per cell is 90 degrees and the linear aperture is for particles with $\delta = 10^{-3}$.

coil diameter	# of dipoles per half cell 4	5	6	7
3.5 cm	9.5	9.3	8.4	7.4
4.0 cm	10.4	10.8	10.0[a]	8.9[a]
4.5 cm	11.0	12.3	11.6	10.5
5.0 cm	11.5	13.7	13.2	12.1
6.0 cm	12.0	16.0	16.7	15.6

[a] Extensively checked against tracking with multiple random number seeds.

CHAPTER VI

The Trade-off Curves

As discussed in Chapter III, the needed linear apertures for various cases are shown in Figs. 6 and 7. These linear apertures have been normalized to the CDR calculated linear aperture, and the other cases are scaled to it using the percentage values given in Figs. 6 and 7.

In the previous chapter, we found for the CDR case (60 degrees phase advance, 4 cm coil diameter, and 5 dipoles per half cell) that the on-momentum calculated linear aperture is 9.9 mm. The needed linear apertures for the other cases, obtained by scaling, are given in Tables 3.1 and 3.2.

Table 3.1

Needed linear aperture for various cell structures for on-momentum particles.

Phase Advance Per Cell	# of Dipoles per half cell	needed linear aperture (mm)
60 deg.	4	9.2
	5	9.9 (reference point)
	6	10.7
	7	11.5
90 deg.	4	8.8
	5	9.5
	6	10.1
	7	10.7

Table 3.2

Needed linear aperture for various cell structures and $\delta = 10^{-3}$.

Phase Advance Per Cell	# of Dipoles Per Half Cell	Needed Linear Aperture (mm)
60 deg.	4	6.2
	5	6.7
	6	7.2
	7	7.6
90 deg.	4	5.8
	5	6.2
	6	6.6
	7	7.0

Having established the needed apertures, the trade-off curves between cell length and magnet coil diameter can be found. Take the case of four dipoles per half cell and 60-degree cells. Table 2.1 shows that in order to reach the needed aperture of 9.2 mm for the on-momentum particles, the coil diameter must be $\geq$ 3.47 cm. Similarly Table 2.3 shows that in order to reach 6.2 mm linear aperture at $\delta = 10^{-3}$, the coil diameter has to be $\geq$ 2.8 cm. The more stringent of these conditions then determines the minimum coil diameter that fulfills the linear aperture requirement for the case user study. This procedure is repeated for all cases to produce the trade-off curves shown in Figs. 10.1 and 10.2.

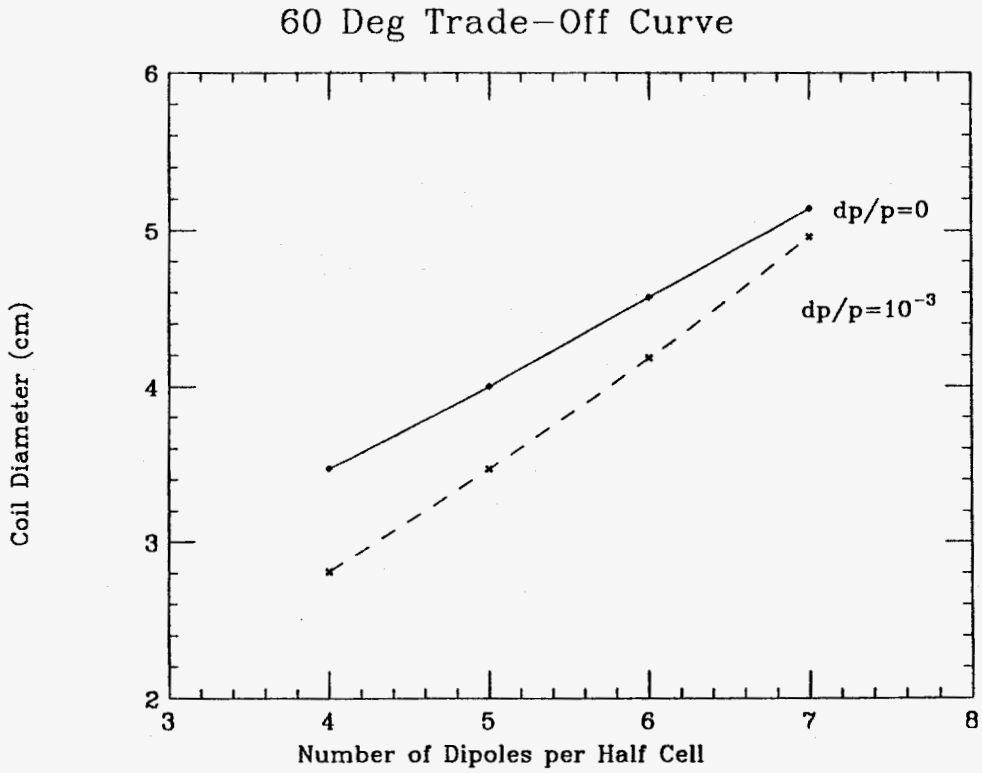

Fig. 10.1 Trade-off curve for the case of 60-degree cells. The solid curve is the result for the on-momentum case. The dotted curve is for the case with $\delta = 10^{-3}$. Below the trade-off curve, the calculated linear aperture is less than the needed one and is thus not acceptable. Since the on-momentum requirement (solid curve) imposes a stronger condition, the net trade-off curve is given by the solid curve.

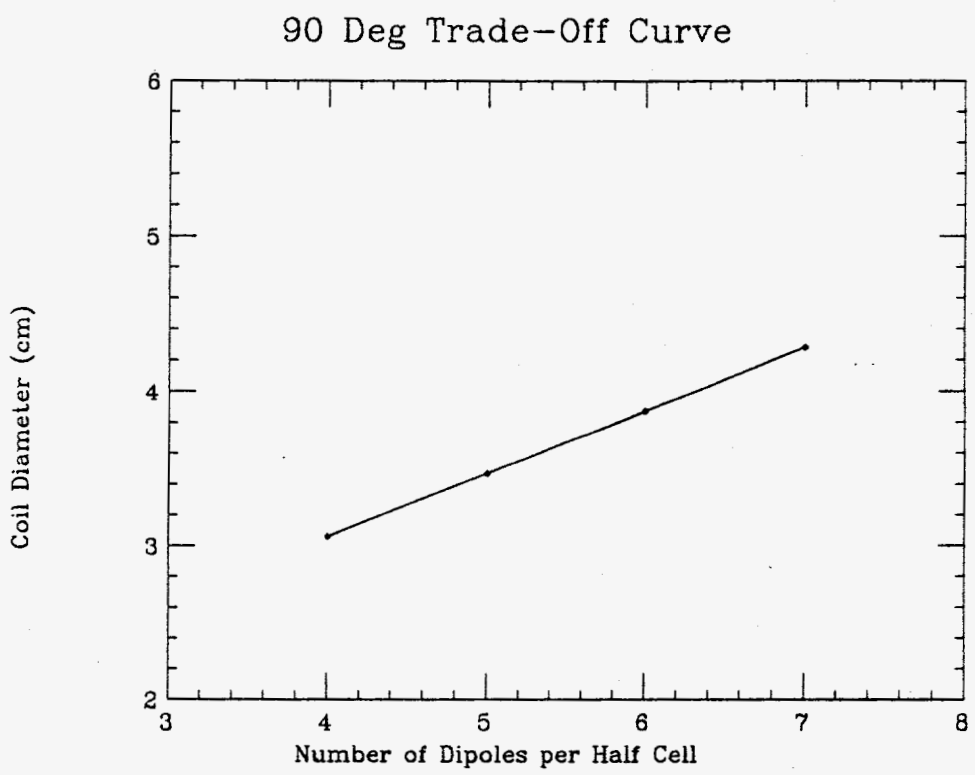

Fig. 10.2 Trade-off curve for the case of 90-degree cells. Only the on-momentum curve is shown. The $\delta = 10^{-3}$ requirement is below the range of d_c being considered and is well-fulfilled.

CHAPTER VII

Cost Model

The input parameters required by the cost model consist of the quadrupole and spool piece lengths and the number of dipoles per half cell. This information defines the cell length and the number of cells, which in turn give the machine circumference (for a fixed IR layout). The magnet coil diameter is the only other additional data needed to define the cost of the machine. Using this input, a program was written to scale the cost information as given in Appendix D of the CDR[1] and to produce the final result. This method relies on the fact that each of the major cost elements can be broken down at the WBS level 5 into a fixed cost, and/or a component that varies with machine circumference (tunnel costs, cryogenic, and power distribution, etc.), and/or a component that depends on the number of half cells (the accelerator interface and control points, number of quadrupoles and spools), and/or a part that depends on the magnet coil diameter.

The relative costs of the magnetic elements as a function of coil diameter d_c were obtained from the Brookhaven Magnet Cost Model.[9] The results of this model are shown in Fig. 11, which gives the percentage change in dipole cost (normalized to $d_c = 4$ cm) as a function of d_c. These results differ only marginally from earlier scaling curves and result in a 10% change in magnet differential costs for a 5 mm change in coil diameter. This curve was applied to the quadrupole and correction elements as well as the dipoles.

The costs calculated in this chapter are the component costs for the machine that amounted to $2000M in the CDR and do not include contingency, system engineering and design, and management and support (WBS elements 3,4, and 5) which amounted to another $1010M. All costs are expressed in $FY86.

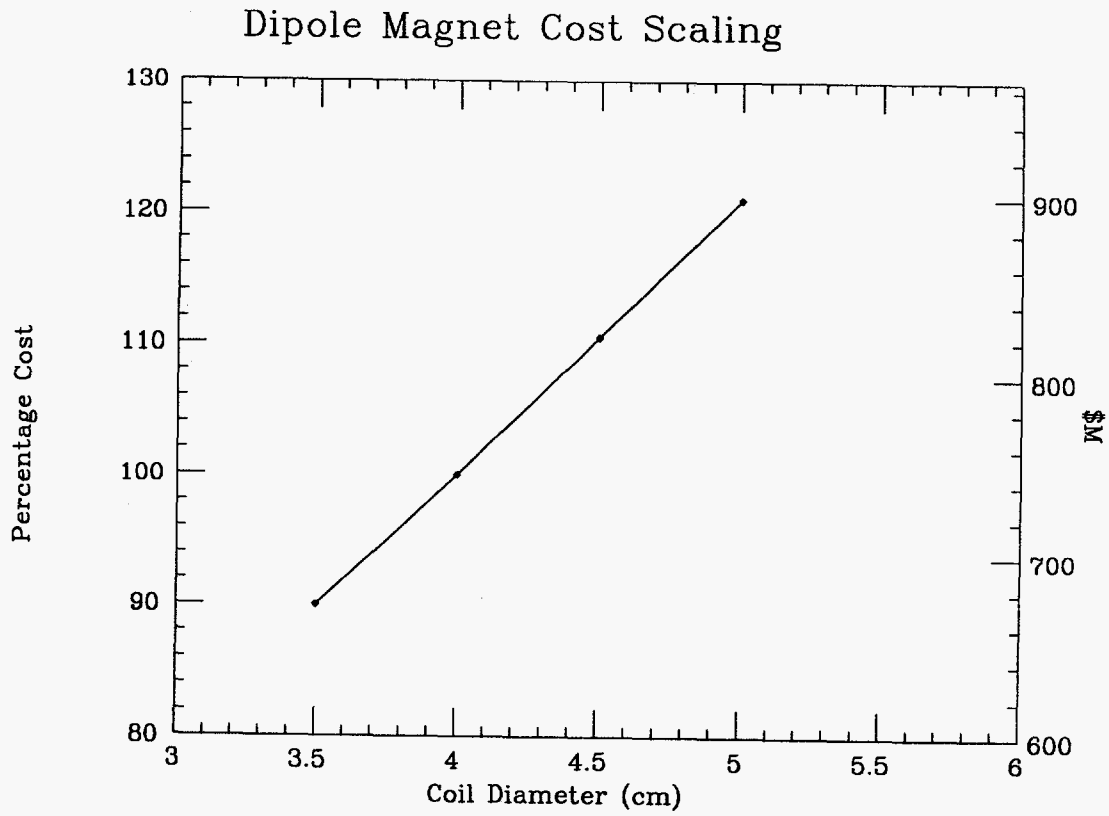

Fig. 11 Dipole costs as a function of dipole coil winding diameter in $M and as a percentage of the CDR dipole costs.

Details of how the major subsystem costs vary with cell parameters are described in Appendix A. The effects of varying the cell length (through the number of dipoles per half cell) and phase advance on the quadrupole and spool piece costs are shown respectively in Figs. 12.1 and 12.2 for a fixed coil diameter of 4 cm. The percentage cost increase incurred by changing the phase advance from 60 to 90 degrees is approximately constant with respect to the cell length; the overall cost, however, is significantly reduced as the cell length is increased. The reason for this is not so much that the price of an individual element is decreased as the cell is lengthened, but rather that the number of elements, 8 quadrupoles, spool pieces, etc., required in the ring is substantially reduced. Thus the cost of increasing the phase advance to 90 degrees per cell can be negated by adding one more dipole to each half cell.

Following the magnets, the largest cost elements are the conventional construction and the cryogenic system. These cost curves are shown in Figs. 12.3 and 12.4. The cryogenic system cost is effectively independent of phase advance; the conventional construction reflects the increased machine circumference more strongly. In both cases the percentage variation is relatively small (~5%) across the range of the parameters considered.

Figures 13.1 and 13.2, show the total component cost (i.e., all the cost elements), as a function of the cell length and coil diameter for both 60- and 90-degree cases. The costs are expressed as a percentage of the 60-degree, 4.0 cm coil diameter, 5 dipoles per half cell lattice used in the CDR. At this point in the parameter space, changing the coil diameter by 5 mm changes the cost by ~5%. Inceasing the phase advance from 60 to 90 degrees costs ~2%, and adding one more dipole to the half cell results in a saving of ~2% for the 60-degree lattice, ~3% for the 90-degree one.

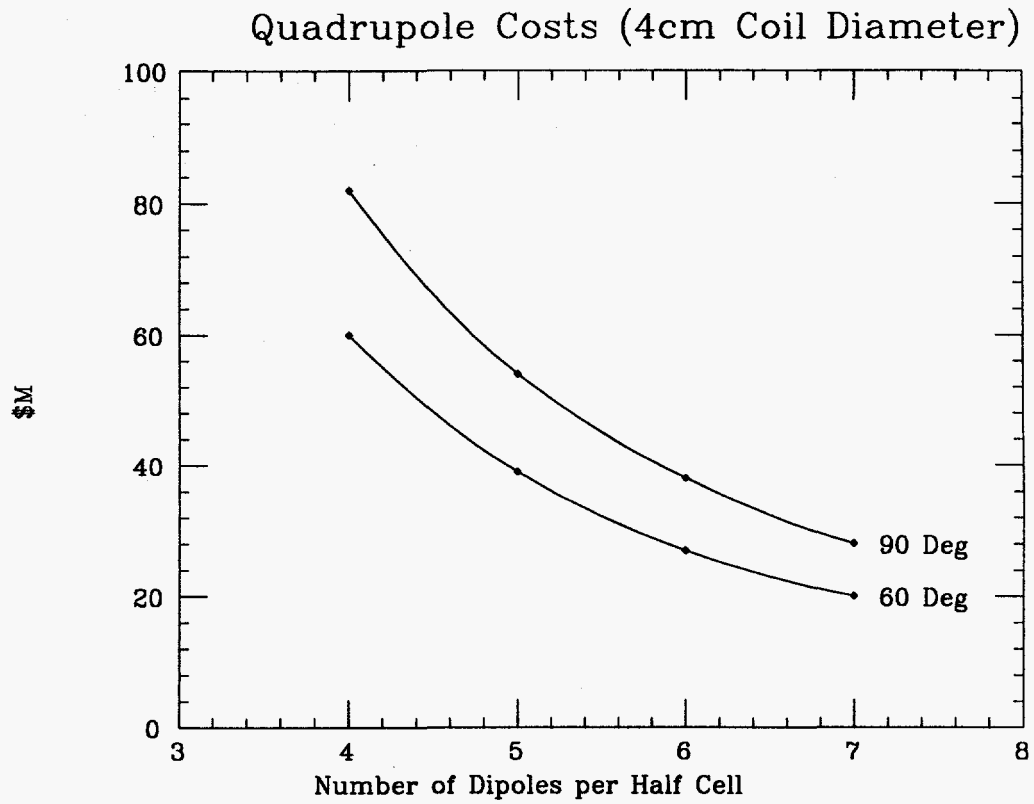

Figure 12.1

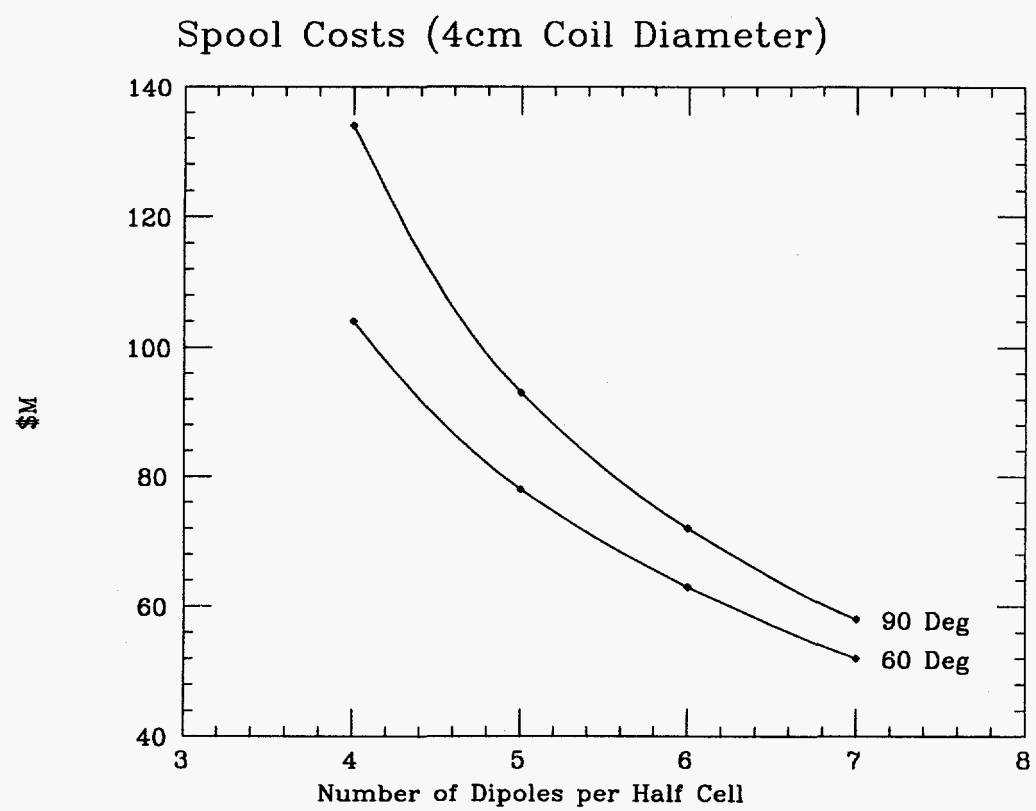

Figure 12.2

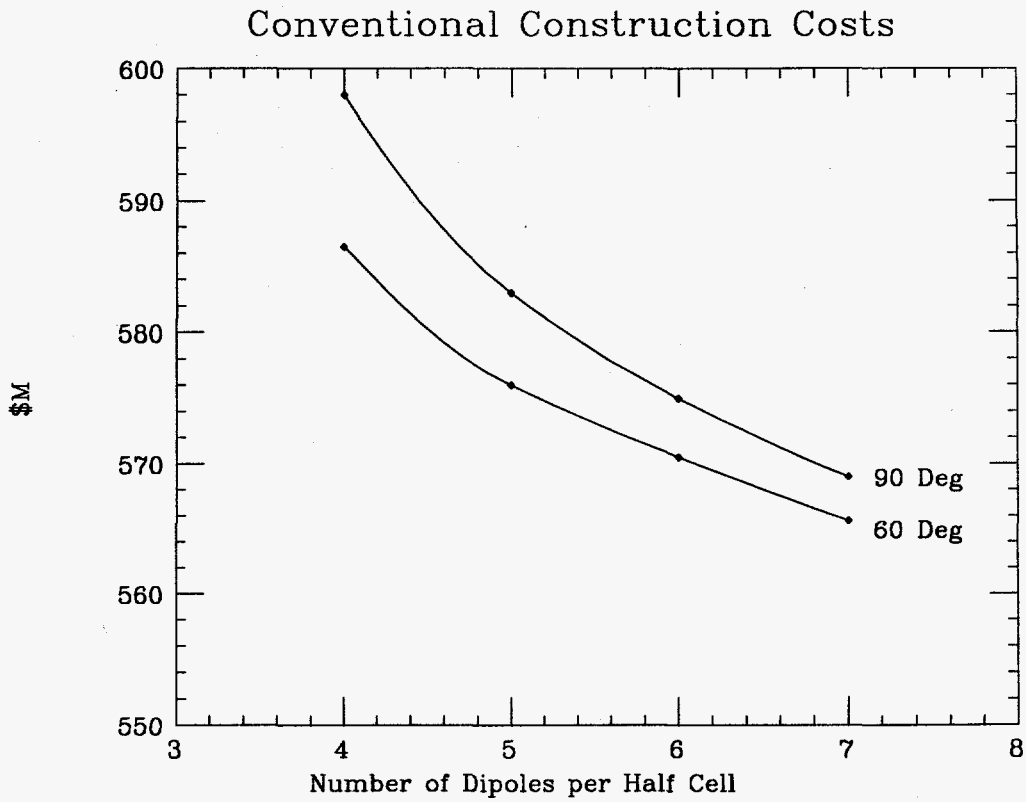

Figure 12.3

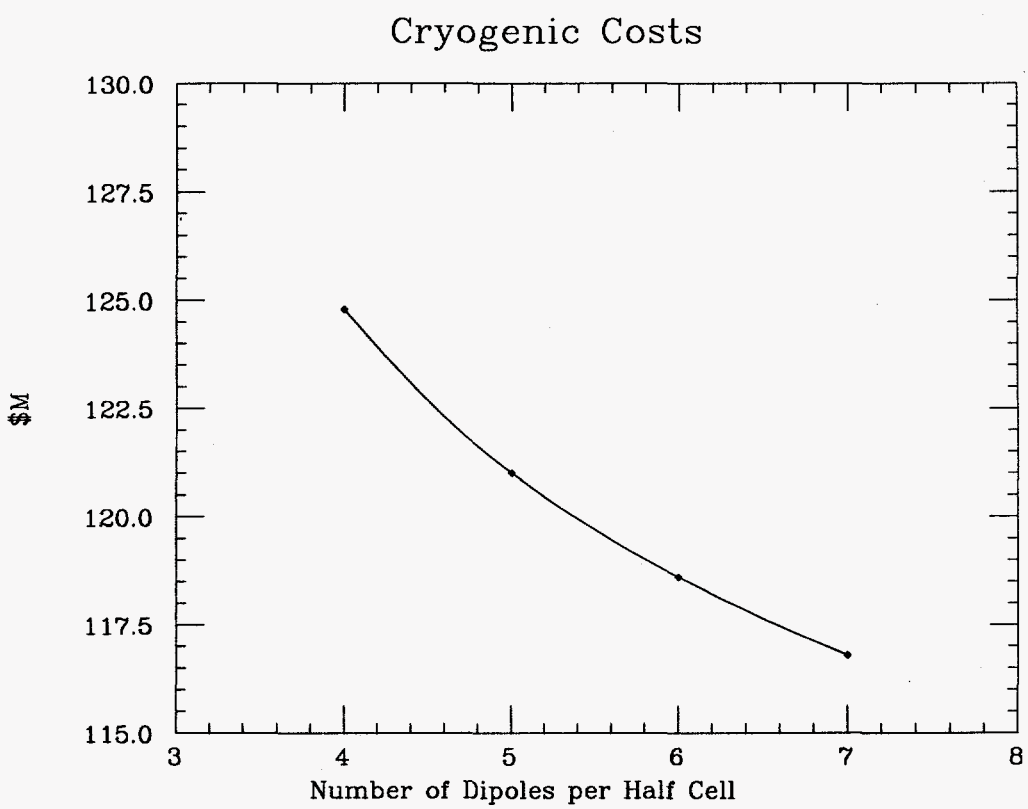

Figure 12.4

Fig. 12.1 - 12.4 Component costs as a function of the number of dipoles per half cell.

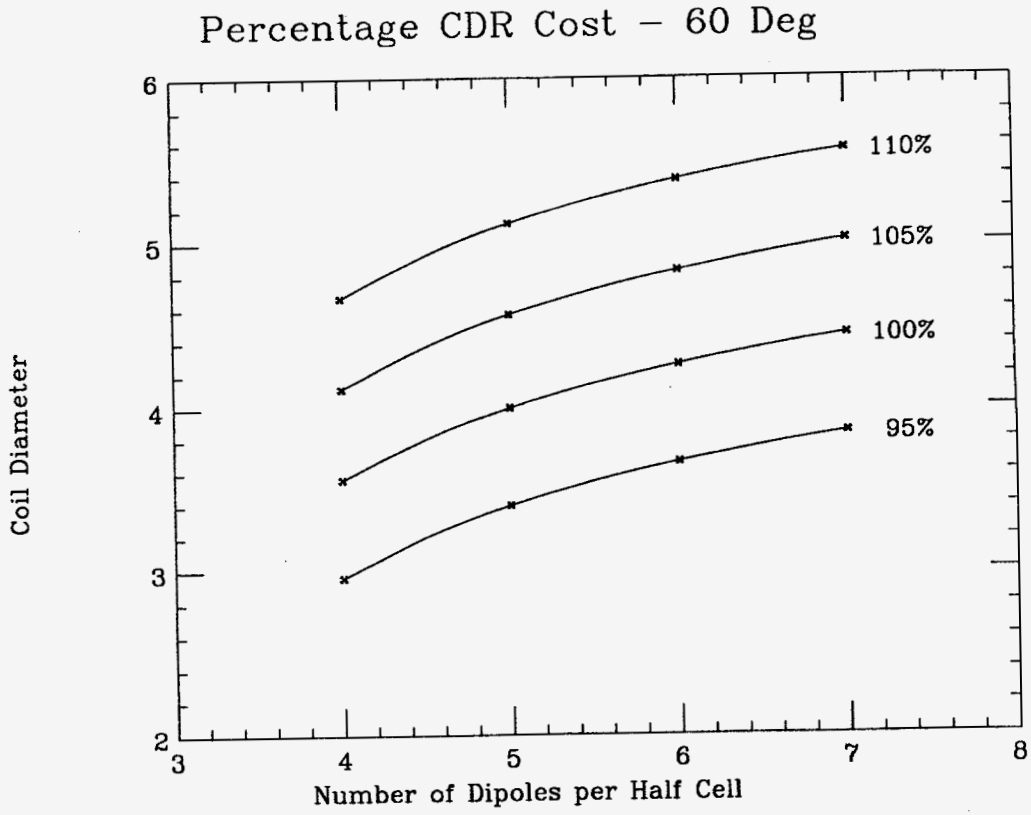

Fig. 13.1 Total component cost contours in percentage of the CDR as a function of the number of dipoles per half cell plotted against the dipole coil winding diameter for 60° cells.

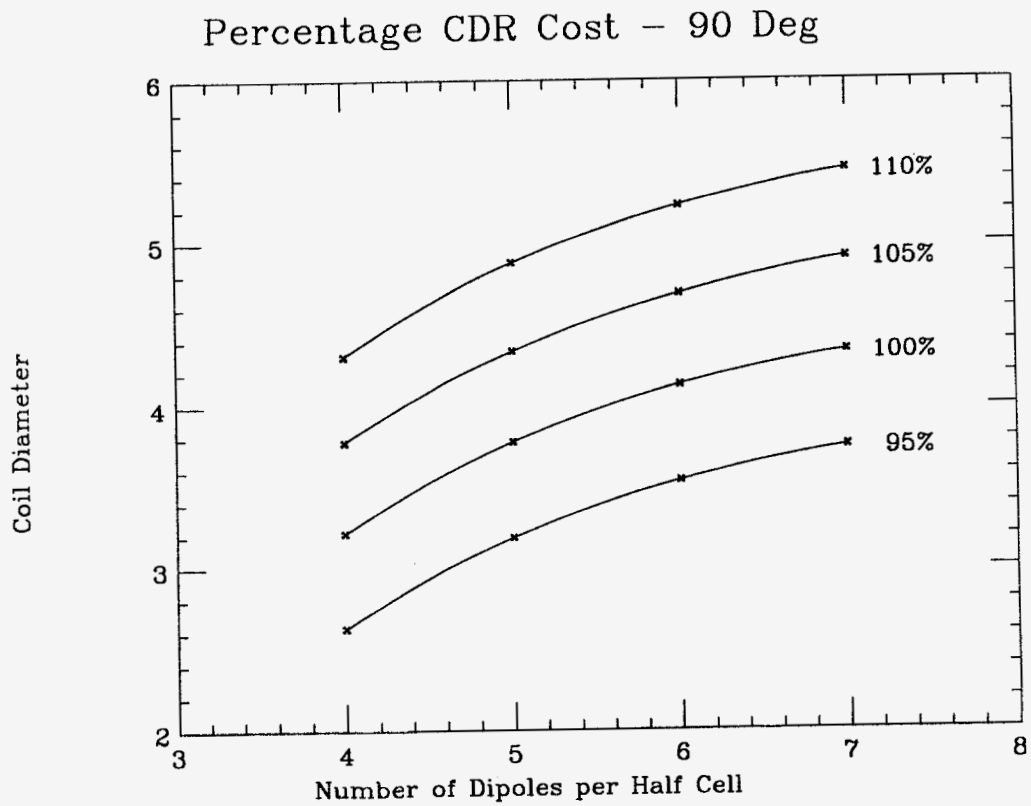

Fig. 13.2 Total component cost contours in percentage of the CDR as a function of the number of dipoles per half cell plotted against the dipole coil winding diameter for 90° cells.

CHAPTER VIII

Additional Considerations

Several issues other than the linear aperture need to be considered. Although they are not the determining issues as far as the cell lattice parameters are concerned, it is important to show that our choice does not cause any unacceptable effects concerning these issues. In this chapter, we will consider these additional effects.

1. Systematic Multipole Tolerances

The tolerance on the systematic magnetic multipoles in the dipole magnets is determined by the betatron tune shifts that they produce. The tune shift $\Delta\nu_n$ produced by the "normal" 2(n+1) multipole coefficient b_n for one-dimensional, horizontal motion is given by

$$\Delta\nu_n = \beta b_n < (\eta\delta + A_\beta \cos\phi)^n \cos\phi > /A_\beta \quad , \tag{8}$$

where β is the horizontal beta function, η the dispersion function, δ the fractional energy deviation, and A_β the betatron amplitude. The brackets indicate an average over ϕ, and the whole expression is to be averaged over the lattice.

The lattice parameters affect the tune shift through the β and η functions and also through the betatron amplitude. The <u>total</u> tune shift produced by all of the systematic multipoles is the sum over n of all the contributions $\Delta\nu_n$. Since the relative values and signs of the b_n are not known, we estimate the b_n tolerances individually by the criterion that $\Delta\nu_n < 0.005$ at betatron amplitudes that are roughly $\sqrt{2}$ larger than the required linear apertures, both on-momentum and at $\delta = 10^{-3}$, for the CDR lattice. The betatron amplitude is 7 mm at β_{max} at $\delta = 0$ and 5 mm at $\delta = 10^{-3}$. For the other lattices, the amplitudes used are scaled relative to

these CDR values from the respective needed linear apertures at $\delta = 0$ and $\delta = 10^{-3}$ using Figs. 6 and 7. The amplitudes that enter the $\Delta\nu_n$ formula are these corresponding to the average value of the respective betatron functions β. The lattice parameters and average betatron amplitudes used are tabulated in Table 4.

Table 4

Lattice Parameters
(N = number of dipoles per half cell)

N	μ	L	β	η	$A_\beta(\delta = 0)$	$A_\beta(\delta = 10^{-3})$
4	60°	79.9m	185m	2.09m	5.25mm	3.78mm
5	60°	96.0	222	3.14	5.72	4.09
6	60°	112.6	260	4.42	6.19	4.43
7	60°	129.4	299	5.93	6.66	4.78
4	90°	83.3	166	1.09	4.74	3.33
5	90°	98.5	197	1.61	5.12	3.56
6	90°	114.5	229	2.25	5.48	3.80
7	90°	130.9	262	3.00	5.85	4.04

The resulting tolerances on the systematic multipole coefficients (in units of 10^{-4} of the dipole field at 1 cm) are tabulated in Table 5. (Since for even-n $\Delta\nu_n$ is proportional to δ, no realistic tolerance for even-n b_n can be derived in this approximation at $\delta = 0$.)

The smaller tolerances in each case are plotted in Fig. 14. In addition, a band of "anticipated" values of non-allowed systematic multipoles for the SSC dipoles is indicated. These "anticipated" values were simply scaled from the average values of the non-allowed multipoles observed in the Tevatron dipoles. The average values of the non-allowed multipoles in the first long SSC dipole (D0001) are not inconsistent with this band of values.[10] Also indicated are the anticipated persistent-current multipole strengths at injection for n = 4,6,8, and 10 for the 4-cm coil i.d.

Table 5

Systematic Multipole Tolerances

Units: Strength at 1 cm relative to dipole field x 10^{-4}

At $\delta=0$:

N	μ	b_1	b_2	b_3	b_4	b_5	b_6	b_7	b_8
4	60°	.0054	--	.026	--	.11	--	.47	--
5	60°	.0045	--	.018	--	.067	--	.23	--
6	60°	.0039	--	.013	--	.042	--	.12	--
7	60°	.0033	--	.010	--	.027	--	.069	--
4	90°	.0060	--	.031	--	.140	--	.64	--
5	90°	.0051	--	.023	--	.091	--	.35	--
6	90°	.0044	--	.017	--	.060	--	.20	--
7	90°	.0038	--	.013	--	.040	--	.12	--

At $\delta=10^{-3}$:

4	60°	.0054	.013	.023	.043	.080	.15	.26	.48
5	60°	.0045	.0072	.011	.016	.024	.035	.051	.074
6	60°	.0039	.0044	.0052	.0064	.0077	.0092	.011	.13
7	60°	.0033	.0028	.0027	.0027	.0027	.0026	.0026	.0025
4	90°	.0060	.028	.051	.15	.33	.83	2.0	4.7
5	90°	.0051	.016	.029	.065	.13	.28	.57	1.2
6	90°	.0044	.010	.017	.031	.054	.10	.17	.29
7	90°	.0038	.0064	.010	.015	.023	.034	.052	.077

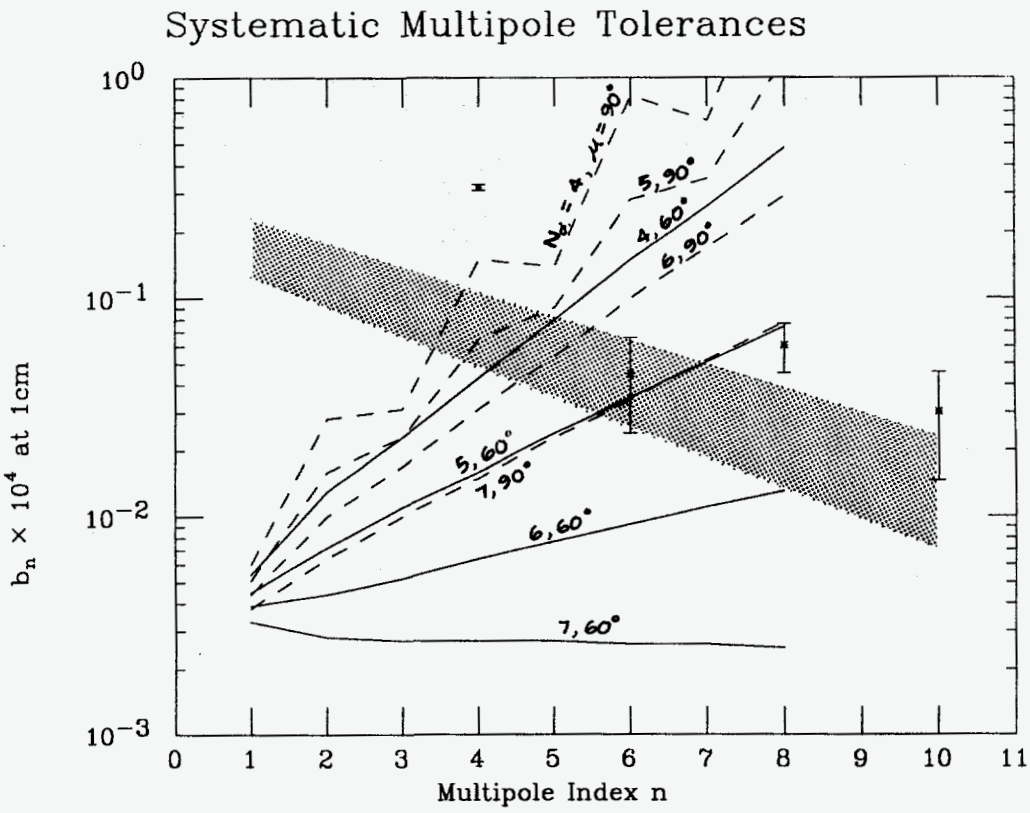

Fig. 14 Systematic normal multipole strengths in the dipole magnet tolerated by lattices having 4 to 7 dipoles per half cell and either 60° or 90° phase shift per cell. Also indicated is the band of systematic non-allowed multipoles anticipated for the SSC on the basis of TEVATRON experience. Also shown are the systematic multipole strengths at injection for n = 4, 6, 8, and 10 due to persistent currents for 5-micron filaments in a 4-cm i.d. coil. [The b_2 persistent current strength is off-scale (about 5 units).]

In conclusion, we find the following:

1) The 90° lattices are more tolerant than the 60° lattices. The short-cell lattices are more tolerant than the long-cell lattices. The total spread in tolerances is only a factor of 2 at n = 1 and a factor of almost 2,000 at n = 8. Qualitatively, this behavior is understandable in terms of the relative values of the dispersion and betatron functions listed in Table 4.

2) A practical conclusion from Fig. 14 is that the number of potentially needed correction circuits is strongly affected by the lattice parameters. Using the indicated band of anticipated multipole strengths due both to geometric effects (scaled from the Tevatron data) and to persistent currents at injection, one concludes that correction circuits will be

needed only up to n = 4 for the best case (N = 4, μ = 90°) and up to n > 11 for the worst (N = 7, μ = 60°), as listed in Table 6 for four values of coil diameter. Better data on the systematic multipole values in the SSC dipoles will be needed before the exact number of required circuits can be determined.

Table 6

Maximum order of systematic multipole potentially requiring correction (N = number of dipoles per half cell)

N	μ	d_c = 3.5	4.0	4.5	5.0 cm
4	60°	4-5	4-5	4-5	4-5
5	60°	8	5-6	5-6	5-6
6	60°	10	10	8-10	7-10
7	60°	>11	>11	>11	>11
4	90°	4	4	4	3
5	90°	4	4	4	4
6	90°	6	4-5	4-5	4-5
7	90°	8	6	5-6	5-6

2. Impact of Cell Parameters on the IR Lattice

The IR optics are indirectly affected by the lattice parameters, mainly through their influence on the straight-section lengths. The shorter cells, and/or the 90-degree phase advance, permit shorter dispersion suppressors, which in turn permit longer straight sections and/or shorter distance between adjacent interaction points. Longer straight sections allow either lower secondary maxima in the betatron functions, or longer central free-spaces in the medium-beta IRs and the utility straight sections, the latter relaxing the abort requirements.

An additional advantage of shorter straight sections and/or shorter dispersion suppressors is that the cost of providing a by-pass version of IR layout is lower.[11] There are several designs of dispersion suppressors, all of which either automatically provide, or can be modified slightly to provide, enough free space for scrapers and collimators.

The 90-degree cell allows the shortest dispersion suppressor. For example, the 90-degree "short cell" design can be realized in the length of 1.5 normal cells; however, there is a minimum allowable length of dispersion suppressor because of the minimum amount of bend needed to shield one IR from the muons from the adjacent IRs.

In summary, the IR lattice design favors 90-degree cells and, to a lesser extent, short cell length. As an example and an existence proof a 90-degree lattice with six dipole magnets per half cell is described in Appendix B.

3. Impact of Magnet Size on Beam Instabilities and Parasitic Heating[12]

The impedance contributions from rf cavities, vacuum-chamber walls, space charge, bellows, beam collimators (negligible), beam position monitors, injection and abort kickers, and coherent synchrotron radiation were considered as functions of the chamber size.

The vacuum chamber size depends on the magnet coil size. As a result, the magnet coil size affects the impedance seen by the SSC beam. The various sources of impedance have been examined as functions of the vacuum chamber radius. The reactive parts of the transverse impedance sources are listed in Table 7. The total $Im(Z_\perp)$ ranges from 32 to 64 MΩ/m for chamber radii between 1.15 and 2.15 cm (1.65 cm is the nominal CDR value.). The total longitudinal impedance $|Z_\parallel/n|$ is not sensitive to this geometrical change and differs from the CDR value (0.2 ohm) only by 5% over this range.

Single-Bunch Instabilities

The impedance thresholds for single-bunch instabilities are calculated to be[1]

	Long Threshold	Trans. Threshold
Microwave	$\lvert Z_\parallel/n\rvert=15.5\ \Omega$	$\lvert Z_\perp\rvert=590$ MΩ/m
Mode-coupling	$Im(Z_\parallel/n)=87\ \Omega$	$Im(Z_\perp)=250$ MΩ/m

Thus the SSC is well below threshold for the single-bunch instabilities.

Table 7

Low Frequency Reactive Parts of $Z_\perp$ (in MΩ/m) for different chamber radii b (in cm)

	b=1.15	1.4	1.65	1.9	2.15
Space charge	21	21	21	21	21
Bellows	20	12	7	4.5	3.2
Kickers	1.4	1.4	1.4	1.4	1.4
BPMs	22	15	11	8.3	6.5
Total	64	49	39	35	32

Multi-Bunch Instabilities

As noted in the CDR, the growth rates of the coupled bunch instabilities, both longitudinal and transverse, are almost exclusively determined by the higher order parasitic modes of the rf cavity cells. Since these modes are insensitive to the size of the vacuum chamber fitting into the rf cavity noses, the growth rates are almost unaffected by a change in chamber radius up to ± 0.5 cm and the CDR values remains intact.

The only exception to the above statement is the transverse dipole modes due to resistive wall at low frequency. This is because the transverse impedance $Z_\perp(\omega)$ for resistive wall peaks sharply like $\omega^{-1/2}$ as $\omega \to 0$ and its strength increases as b^{-3} for decreasing radius b. As discussed in the CDR, we need a feedback system to damp these unstable modes in any case. The gain of the feedback loop required may have to be increased by a factor of $(b_0/b)^3$, or about three for the worst case b = 1.15 cm. However, the bandwidth of this feedback system to damp the resistive wall is quite narrow (comparable to revolution frequency); the increase of gain does not impose a significant problem.

The real frequency shifts of the transverse modes are determined by the low frequency reactive parts of $Z_\perp$. In general, these shifts increase

linearly with $Im(Z_\perp)$. From Table 7, we expect that the frequency shifts increase by ~50% for the worst case b = 1.15 cm. For this case, Landau damping for all nonrigid transverse modes can be insured by either increasing the momentum spread $\Delta p/p$ by 20%, or by increasing the betatron tune spread to twice the CDR value (10^{-4}). These mild modifications to the stability requirements can be met should the smaller chamber be adopted.

The real frequency shifts of the longitudinal modes are determined by the low frequency reactive parts of $Z_\parallel/n$. However, the total $Z_\parallel/n$ is rather insensitive to the change of vacuum chamber radius. Therefore, the CDR conclusions for the longitudinal instabilities remain valid--namely that all modes, except the dipole mode (n = 1) at 1 TeV, are Landau damped with $\Delta p/p = 1.75 \times 10^{-4}$. The unstable dipole mode at 1 TeV either needs a feedback system, or can be Landau damped as well by a larger $\Delta p/p = 2 \times 10^{-4}$, as recently suggested by Zotter.[13]

Parasitic Heating

The impact of varying the radius of the vacuum chamber on the parasitic heating in the cryogenic regions of the storage rings can be summarized by the formula[12]

$$P = 320 + 524\, b_o/b \quad \text{(watts, total for both rings)} \tag{9}$$

The parasitic heating varies from 0.72 kW at a chamber radius of 2.15 cm to 1.1 kW at 1.15 cm. Thus there is no significant change in the cryogenic load over this range of chamber size from that given in the CDR (0.9 kW). The parasitic heating in the rf cavities and in the kicker magnets stay with their CDR values; they are not included in Eq. (9) because those components are in the warm-bore regions of the rings.

To summarize the impact of vacuum chamber radius on instability and parasitic heating, we found that these effects favor larger chambers. Over the range considered, however, no effects are sufficiently strong to perturb the CDR design specifications.

CHAPTER IX

Conclusion

Conclusions are drawn from the trade-off curves, shown in Figs. 10.1 and 10.2, and the cost contour curves, shown in Figs. 13.1 and 13.2. They are readily obtained by superimposing these figures, as shown in Figs. 15.1 and 15.2. The design with minimum cost along the trade-off curves is, in principle, the optimal design and the one for which we are looking.

We first discuss the case with 60-degree cells. Figure 15.1 indicates that the CDR case is very close to being the optimum, i.e., we have as one possible SSC design:

Case 1 (the CDR case): 60-degree cells, 5 dipoles per half cell, 4 cm coil diameter, cost = 100% by definition.

However, Fig. 15.1 shows another possibility, i.e.,

Case 2: 60-degree cells, 4 dipoles per half cell, 3.47 cm coil diameter, cost = 99.34%.

Strictly from these analyses, Case 2 is found to be cheaper than the CDR case by about $13.2M. It is believed that the cost contours are accurate to this level or better. Note that Case 2 involved additional cost (not included in the cost model) for the development of a different dipole magnet design with a 3.47 cm coil diameter.

Similarly from Fig. 15.2, we find two more possibilities:

Case 3: 90-degree cells, 5 dipoles per half cell, 3.47 cm coil diameter, cost = 97.39%.

Case 4: 90-degree cells, 6 dipoles per half cell, 3.87 cm coil diameter, cost = 97.83%.

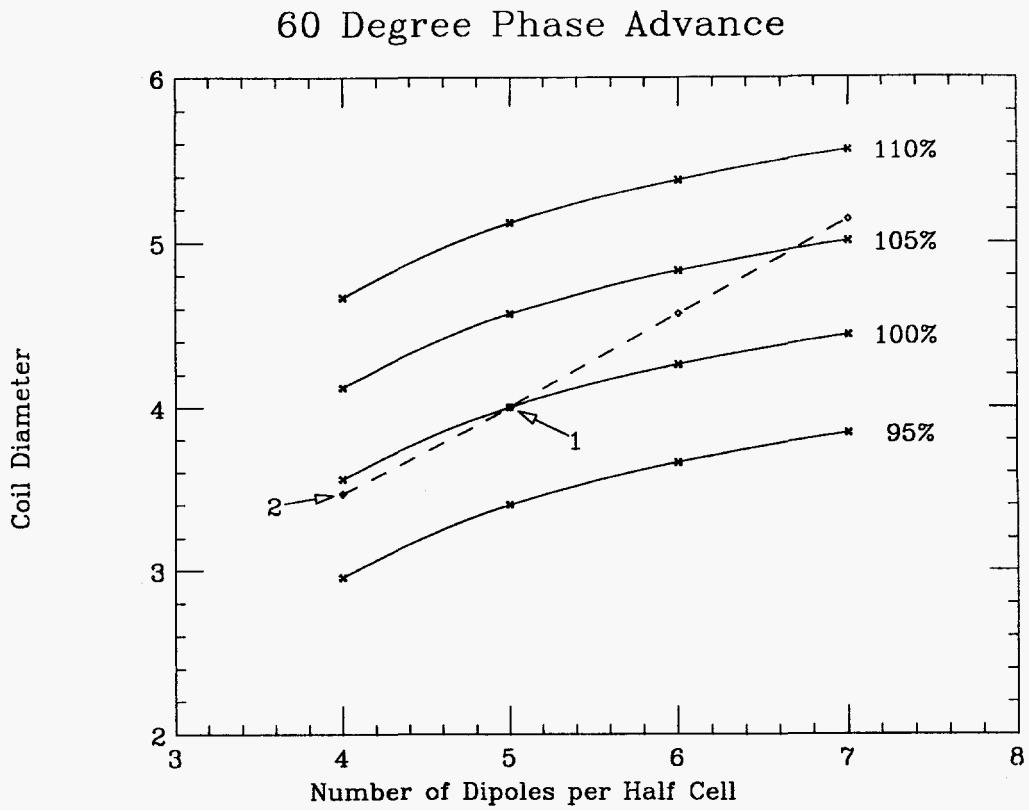

Figure 15.1

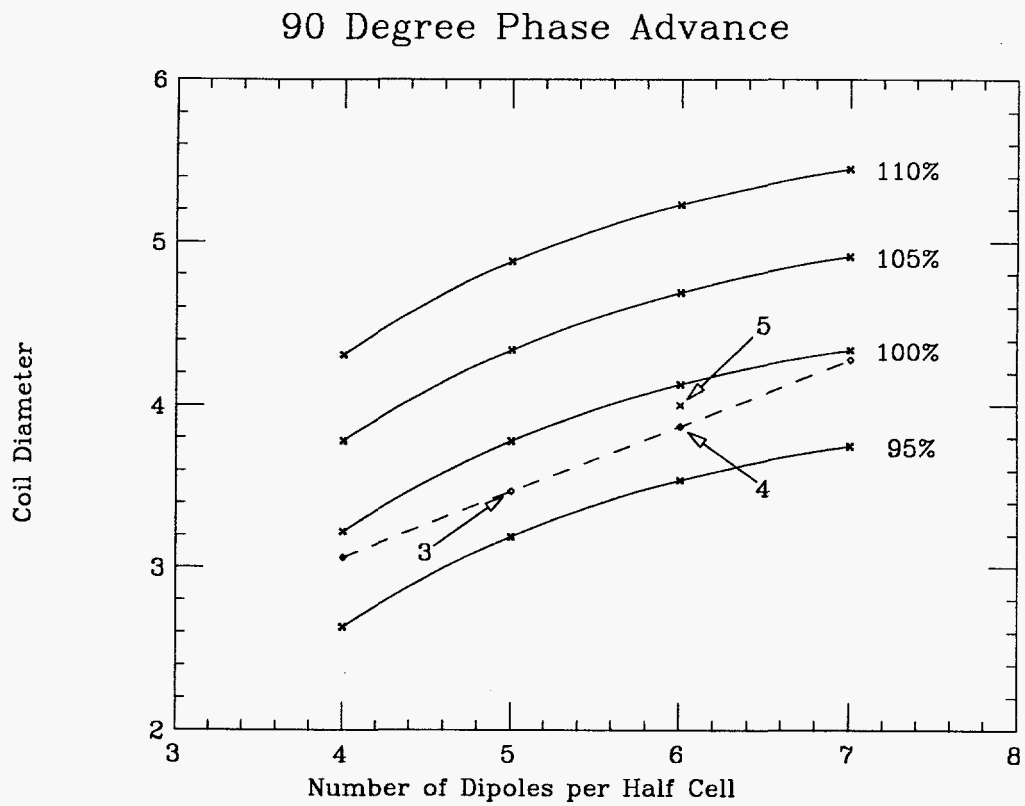

Figure 15.2

Fig. 15.1 and 15.2 Trade-off curve overlaid on total cost curves for 60° and 90° cells. Cases 1-5 are indicated on the plots.

Cases 3 and 4 offer the possibility of substantial savings of $52.2M and $43.5M, respectively, with respect to the CDR case. The cost difference between them is about that of the accuracy of the cost model, and either one will be a strong candidate for our recommended configuration. However, taking into account the effort and expense required to develop new dipole designs, the case that the study group recommends is

Case 5 (the recommended case): 90-degree cells, 6 dipoles per half cell, 4 cm coil diameter, cost = 98.96%.

Note that Case 5 is above the trade-off curve for 90-degree cells. Compared with the CDR case, Case 5 has the following advantages:

(1) It has a potential cost savings of $20.9M.

(2) It has the same magnet coil diameter and therefore no additional development to be performed on dipole magnet design.

(3) The expected linear aperture exceeds the needed linear aperture by 4% (with the normalization that the CDR case has exactly the same expected and needed linear apertures). This means 4% more safety margin than the CDR case. Figure 16 gives the calculated linear aperture of Case 5 as a function of $\Delta E/E$. Also shown are data of linear and dynamic apertures obtained by tracking.

(4) The systematic multipole tolerances are more relaxed, as shown in Fig. 14. If, as a result, fewer correction circuits are required, this will add to the potential cost saving relative to the CDR case.

(5) It allows the possibility of shortening the distance between adjacent interaction regions in the IR clusters.

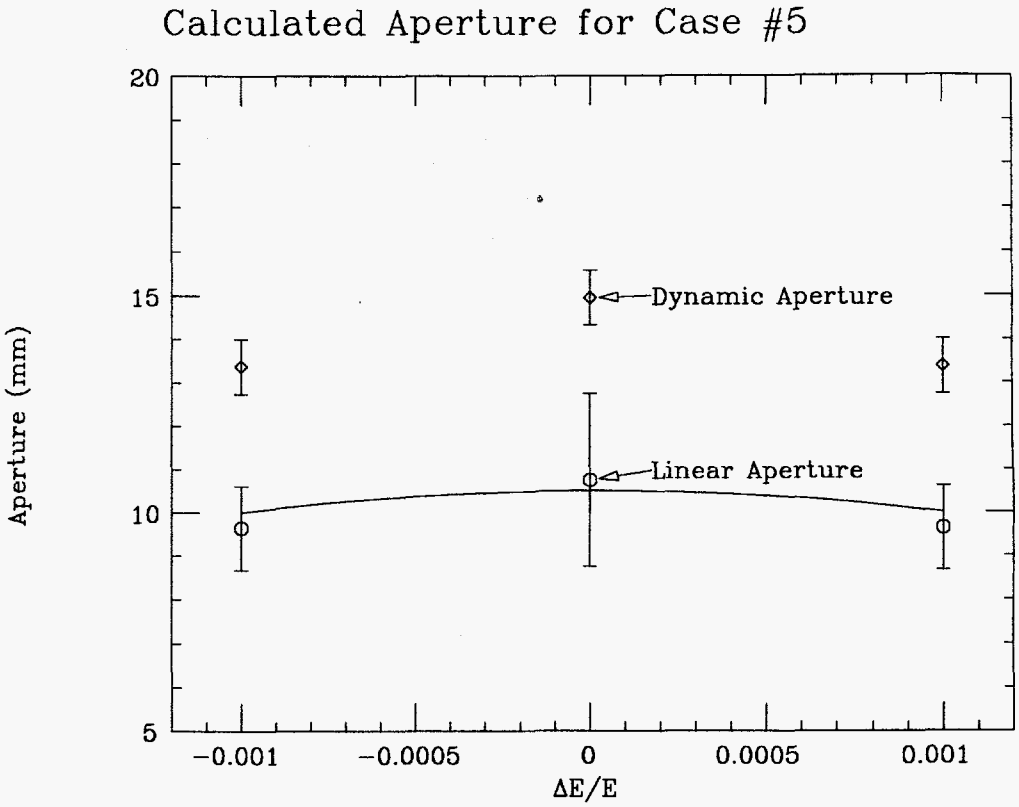

Fig. 16 Calculated linear aperture for Case 5 as a function of ΔE/E. Also shown are data of linear and dynamic apertures obtained by tracking.

APPENDIX A. DETAILS OF THE COST MODEL

The cost model described in Chapter VII assumes the following cost scaling for the SSC major subsystems (all cost numbers in parentheses are for the CDR case):

1) The Injector cost ($189M) is constant.
2) The dipole magnet costs ($746M) are constant with respect to the lattice parameters and vary with coil diameter as shown in Fig. 11.
3) The unit cost of the arc quadrupoles ($29K) varies linearly with the quadrupole length and scales with coil diameter. This unit cost is then multiplied by the number of half cells to get the total quadrupole costs.
4) The unit costs of the spool piece assemblies ($43.4K) are dominated by a fixed cost of $35.9K which contains the cryogenic plumbing, power leads, correction element leads, cryogenic and vacuum instrumentation and controls, and end assemblies. The correction element part of the spool piece costs ($7.5K) vary linearly with length and scale with coil diameter. The primary and secondary spool pieces are treated in an identical fashion. The total cost of the spool piece assemblies is given by the unit cost multiplied by the total number of spool pieces. The number of secondary spool pieces is constant, the number of primary spools is defined by the number of half cells.
5) The magnet tooling costs ($56M) independent of the lattice parameters and assumed to vary by 2.5% for each 5 mm change in coil diameter.
6) The Interaction Region magnet costs ($39M) are independent of the cell parameters and scale with magnet coil diameter.

7) The magnet installation costs ($42.5M) vary linearly with the total number of machine elements, where a machine element is defined as a dipole, a quadrupole, or a spool piece.

8) The cryogenic system costs have been estimated[14] assuming that the number of amperes of superconducting magnet current of all types remains constant. The various components of the total include a fixed cost of $50M (refrigerator stations excluding compressors, transfer line modules, IR regions, magnet testing station), a fraction ($53.7M) which varies slowly with the number of half cells (compressor size and liquid nitrogen plants), a portion ($7.5M) which varies almost linearly with machine circumference (gas distribution system), and a portion ($9.8M) which varies linearly with the number of half cells (instrumentation and controls).

9) The vacuum costs are given by a fixed cost of $5.5M (IR regions and warm beam tube areas such as injection lines), a component which varies linearly with the circumference (cold beam tube, $3.1M), and a portion which is proportional to the number of half cells (insulating vacuum and support services $8.7M).

10) The main power supplies and quench protection systems comprise a fixed cost (main supplies and software, $8.7M) and components that vary linearly with the number of half cells (detection, bypass, and energy extraction systems, $17.8M).

11) The correction element power supplies consist of a fixed cost (the series circuits and the secondary elements, $3.7M) and the correction dipole supplies ($3.1M) which vary with the number of half cells.

12) The beam instrumentation (position detectors and loss monitors, $12.2M) vary with the number of half cells; the profile measuring devices stay fixed ($0.6M).

13) The major costs of the control system (host and sector computers, consoles, and software, $13.5M) stay fixed; the tunnel interface crates ($3.7M) are proportional to the number of half cells; the ring information network ($1.6M) varies with the machine circumference.

14) The personnel safety system in the tunnel varies with the machine circumference ($2.1M), the access, control, and above-ground monitoring stays fixed ($2.7M).

15) The injection ($5.2M), abort ($9.7M), rf ($7.3M), and beam feedback ($4.3M) systems stay the same.

16) The fixed cost overhead in the Conventional Facilities is given by the site and infrastructure ($85.3M), the Campus area ($42.9M), the Injector ($39.7M), and the East and West cluster regions ($72.1M), the surface buildings ($1.7M), the cryogenic facilities ($13.75M), and the experimental areas ($61.4M). The change in costs associated with varying the machine circumference were then calculated by averaging the north and south arc costs ($260M) to obtain an average cost per unit length of tunnel, utilities, and alcoves. This average cost was then multiplied by the new arc length to obtain the final result.

APPENDIX B. EXAMPLE OF A 90° CELL SSC LATTICE

In this appendix, an SSC lattice, based on 90 cells, will be described. As mentioned in the text, the 90° cells offer the possibility of improvements of the IR module design over that of the CDR.

The lattice has two clusters of straight sections connected by two nearly semicircular arcs. Each cluster contains four straight sections with intervening bending sections, while each arc contains 143 regular cells. As in the CDR, each cluster contains four modules of identical length and horizontal bending, and the types of modules are the same, i.e., two utility and two low-β modules in the west cluster, and two utility-type future IR and two low-β modules in the east cluster.

The main parameters of the lattice are given in Table B1. Below we describe the components that enter into this lattice design.

Arc Cells

Each 114 meter half-cell contains six 16.54 m, 6.61 tesla dipoles (at 20 TeV) with 0.8 m separations, one 3.96 m, 211.4 T/m quadrupole, and one 6.0 m correction spool (magnetic effective lengths).

Cluster Modules

The modules have a generic structure, illustrated in Figs. B1 and B2, which show the module that contains a low-β IR. Every module consists of five blocks: a normal half-cell, a dispersion suppressor, a (horizontally) straight section, another dispersion suppressor, and a normal full cell. Corresponding suppressors in each module are identical, 342 m long, compared to 576 m in the CDR and every straight section is 1254 m long, compared to 1152 m, so that the total module length is 2280 meters, compared to 2400 meters.

Table B1

Parameters of 90° Cell SSC Lattice

Circumference	83.448		km
Structure: 2 arcs, 2 clusters			
East cluster modules: 2 utility, 2 medium-β			
West cluster modules: 2 utility, 2 low-β			
Cell phase advance	90°		
Betatron tunes ν_x, ν_y	94.41	94.40	
Short IR, long IR, utility module tunes	3.75	3.25	2.25
β_{max}, β_{min} in arc	388	67	m
η_{max}, η_{min} in arc	3.03	1.45	m
collision, injection β^* in short IR	0.5	13.4	m
collision, injection β_{max} in short IR	8.27	0.67	km
Lengths about IP in short IR	±20		m
IP-IP distance, bending angle	2280	82	m, mrad
Crossing angle range	75 ...	150	μrad
Cells/arc, modules/cluster	143	4	
Cell, cluster module lengths	228	2280	m
Number dipoles per half-cell	6		
Cell, dispersion suppressor dipoles per ring	3576	256	
Magnet field, gradient	6.61	211.4	T, T/m
Average, magnetic radius	13.281	10.085	km
Cell, dispersion suppressor dipole lengths	16.54	16.4854	m
Cell quadrupole length	3.96		m
Vertical beam line separation	0.70		m

The advantage of 90° cells, so far as the insertions are concerned, is that they allow use of shorter dispersion suppressors than 60° cells. As a result, the straight sections can be lengthened without increasing the IP-IP separation. The lengthened straight sections lead to much smaller secondary beta function maxima in the M = -1 channels. In addition, the space available for detectors in the medium-β and "future" IRs can be increased above the ±102 m of the CDR.

Dispersion Suppressors

Each suppressor, see Figs. B1 and B2, consists of two 3/4 length, 90° cells with four rather than six dipoles per half-cell. These dipoles are slightly shorter than regular ones. The length and bending of these cells is such that their dispersion is just half that of the arc cells. As a result the dispersion in them makes half a betatron oscillation about their proper value $\eta_c/2$, from η_c to zero.

With thin lens approximations, $\eta = L\theta$, where L and θ are the half-cell length and bend angle, so in the suppressor cells we want $L\theta = (L\theta)_c/2$. With the choices $L = (3/4)L_c$, $\theta = (2/3)\theta_c$, the suppressor cells are less densely packed with dipoles than the arc cells, so there are enlarged drift spaces next to the quadrupoles for scrapers, beam monitors, etc.

Straight Sections

The three types of modules are distinguished by their straight sections. In this note we will confine ourselves to the low-β IRs.

The design of these straight sections is similar to that in the CDR, but there are four changes: in the total length, the M = -1 channels, the vertical bends, and the matching sections at the ends.

The straight sections are longer than those of the CDR. Hence the βs rise more slowly from the outer triplet, Q6, Q5, Q4, to the inner one, Q3, Q2,

Q1, see Fig. B1. Consequently they enter the M = -1 channel with lower values and rise to a lower maximum value.

As before, the M = -1 channel is made of two short 90° cells, but their structure is FOFDOD rather than FODO. This change also contributes to the smaller beta peaks, and leaves an open space at the center of the channel for a special quadrupole Q7, which is used in the injection optics only (see Fig. B3). Being short, it has little effect on the vertical dispersion. The vertical bends of the second step away from the IP invade the outer drift space of the channel, which again helps by bringing the channel closer to Q4.

The added straight section length is entirely in the interval between Q3 and the channel, so the dipoles of the first vertical step can be shortened from 8 to 5 meters each. In the second step, since the beta functions are now relatively low, we use high field dipoles rather than the weaker ones of the CDR. This also reduces the distance between the channel and Q4.

Finally, another quadrupole has been added to the outer matching section, which gives additional flexibility in going from injection to collision optics.

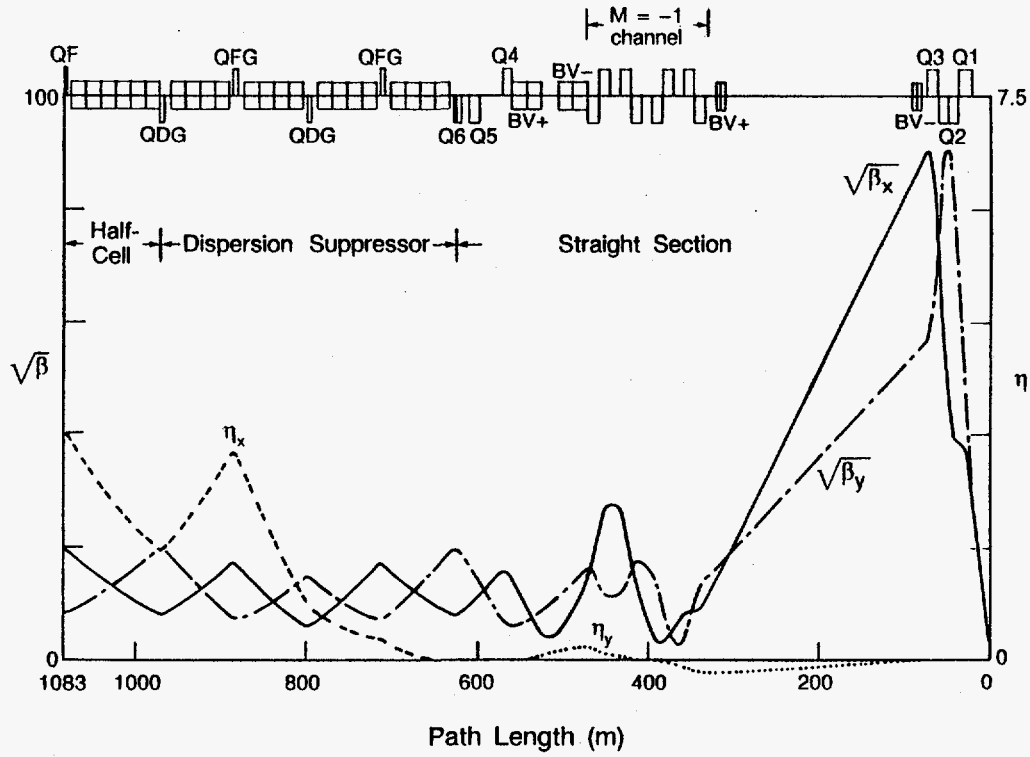

Fig. B1 Left side of 90° Low-β IR module, tuned for collision optics.

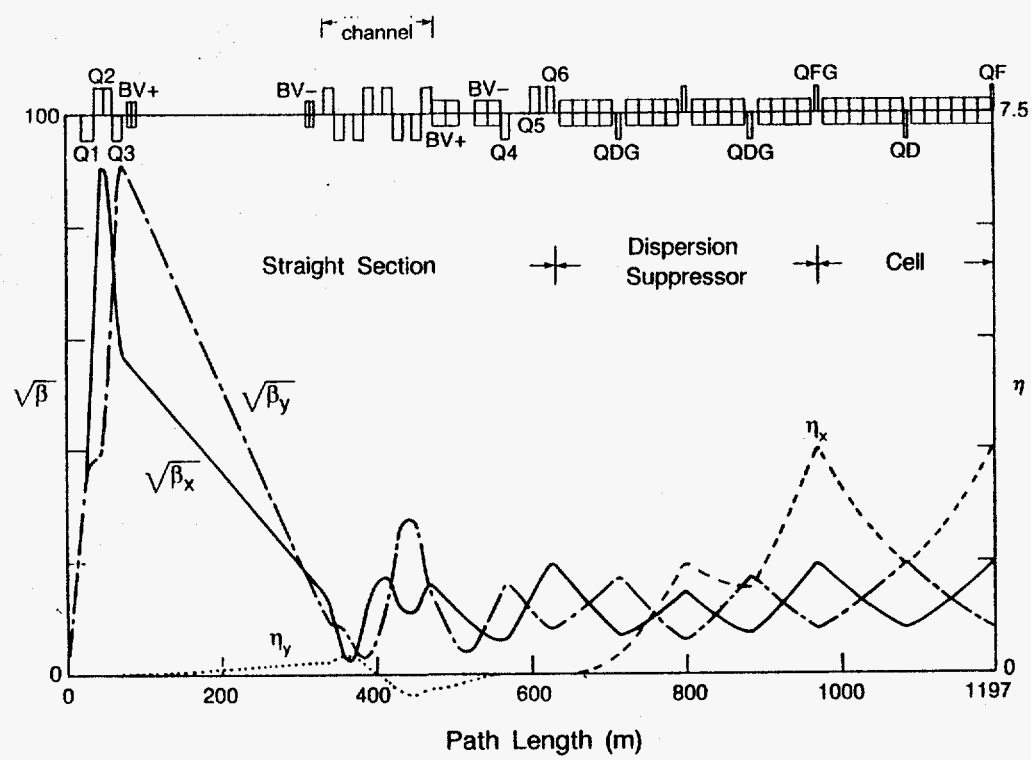

Fig. B2 Right side of 90° Low-β IR module, tuned for collision optics.

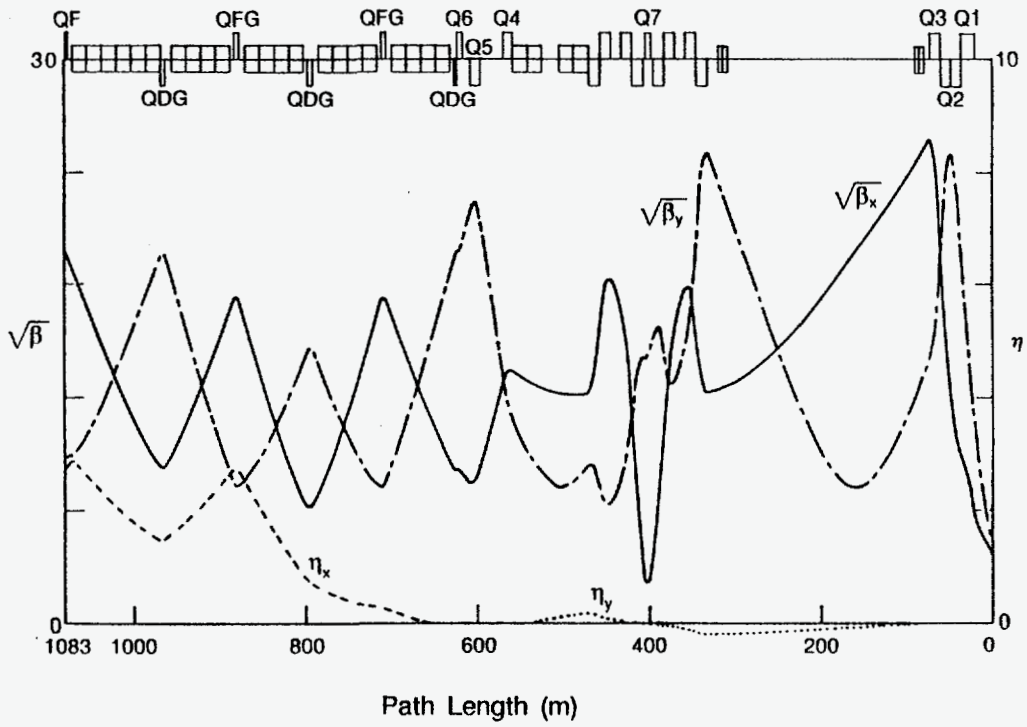

Fig. B3 Left side of 90° Low-β IR module, tuned for injection optics.

References

1. SSC Conceptual Design Report, SSC-SR-2020, March 1986.
2. Aperture Task Force, SSC-SR-1013 (1985).
3. A Chao and E. Forest, SSC-N-81 (1985).
4. Aperture Task Force, SSC-7 (1985).
5. R. Talman, SSC-N-192 (1986).
6. R. Meller, SSC-N-237 (1986).
7. E. Forest, SSC-95, in preparation.
8. B. Leemann and E. Forest, SSC-94, in preparation.
9. K. Goodzeit, private communication (1986).
10. R. Hanft, private communication (1986).
11. SSC IR Layout Task Force, private communication (1986).
12. Abstracted from H. Lee and S. Chattopadhyay, SSC-98 (1986).
13. B. Zotter, SSC-N-230 (1986).
14. M. McAshan, private communication (1986).